Physics of Fluids

RESEARCH ARTICLE | JUNE 26 2024

Statistical analysis of infectious disease transmission risk based on exhaled respiratory droplet trajectory distribution

Marco Cavazzuti ; Paolo Tartarini

Physics of Fluids 36, 063341 (2024)
https://doi.org/10.1063/5.0213041

Physics of Fluids ARTICLE pubs.aip.org/aip/pof

Statistical analysis of infectious disease transmission risk based on exhaled respiratory droplet trajectory distribution

Cite as: Phys. Fluids **36**, 063341 (2024); doi: 10.1063/5.0213041
Submitted: 8 April 2024 · Accepted: 5 June 2024 ·
Published Online: 26 June 2024

Marco Cavazzuti[1,a] and Paolo Tartarini[2]

AFFILIATIONS

[1]Dipartimento di Scienze e Metodi dell'Ingegneria, Università degli Studi di Modena e Reggio Emilia, via Giovanni Amendola 2, Reggio Emilia 42122, Italy
[2]Dipartimento di Ingegneria "Enzo Ferrari," Università degli Studi di Modena e Reggio Emilia, via Pietro Vivarelli 10, Modena 41125, Italy

Note: This paper is part of the special topic, Flow and the Virus.
[a)]**Author to whom correspondence should be addressed:** marco.cavazzuti@unimore.it

ABSTRACT

In the present work, the risk of infectious disease transmission is evaluated based on a statistical analysis of respiratory droplet trajectory distribution. An analytical model recently developed by the authors allows the prediction of the trajectory and evaporation rate of exhaled droplets. The model is used to collect data from a sampling set of more than twenty thousand droplets distributed over a range of diameters from 0.1 μm to 1 mm for different respiratory scenarios. The analytical tool implements the governing equations of droplet transport, evaporation, energy balance, and chemical composition. It also features a two-dimensional unsteady empirical model of respiratory cloud including momentum dissipation and buoyancy. A discrete random walk approach to simulate the droplet turbulent dispersion, and the randomization of the droplet release within the exhalation period and the mouth cross section area complete the model enabling statistical analyses to be rightly performed. With the due boundary conditions, different types of respiratory events can be modeled easily. With additional information on the exhaled droplet size distribution and viral content, spatial maps of virus concentration are derived and associated with the risk of infectious disease transmission being able to discriminate between various transmission routes such as fomite, airborne, or direct inhalation. Different scenarios are presented including mouth breathing, nose breathing, speaking, coughing, and sneezing. The fluid dynamic behavior of respiratory droplets is explored on a size basis, and the role of ventilation discussed. Risk evaluation provides useful information for a knowledgeable discussion on the prevention needs and means from case to case.

I. INTRODUCTION

A primary mean of host-to-host infectious disease transmission is given by pathogen-laden respiratory droplets exhaled while breathing, speaking, coughing, or sneezing. Depending on their size, spanning several orders of magnitude, and the ambient thermohygrometric conditions, droplets can either fall to the ground as they evaporate, or dry out leaving an airborne nucleus made of salts and proteins. Any virus transported by the droplet may survive up to several hours if airborne and up to several days when deposited on surfaces. During this lapse of time it can be transmitted to the airways of a susceptible host either through contact with an infected surface (e.g., fomite route) or through inhalation (e.g., airborne route) fostering the pathogenesis.

The already relatively rich and varied literature on the subject experienced a sudden boost during the most recent SARS-CoV-2 pandemic as many studies tackled the issue from different perspectives.

From a fluid mechanics point of view, a fundamental role over infectious disease transmission is played by the transport and evaporation mechanisms governing the droplet trajectory and ultimately its fate. Trajectory evaluation cannot ignore the presence of the unsteady and intermittent humid air breath cloud within which the droplet is emitted, transported, and protected from evaporation. Further, turbulence induces random velocity fluctuations perturbing the trajectory and favoring droplet dispersion.

Due to the complexity of the physics involved several studies approached the problem numerically using Computational Fluid

Dynamics (CFD) following an Eulerian and/or Lagrangian approach with Discrete Phase Model (DPM) simulations. Most works focus on the analysis of specific indoor scenarios in the presence of a given ventilation strategy. For instance, in Ref. 1, the exhaled droplet dispersion due to speaking in a ventilated office room is investigated using a Lagrangian approach: the impact of different ventilation strategies on droplet dispersion is discussed. In a similar fashion, the role of ventilation in hospital rooms is analyzed in Ref. 2. In Ref. 3, droplet dispersion due to breathing or talking, or following a cough or a sneeze on a bus is dealt with: larger droplets are modeled using a Lagrangian approach, smaller ones with an Eulerian approach. In Ref. 4, the focus switches to a cough in a supermarket aisle whereas different CFD tools are compared over the same scenario. Although these studies are interesting for their practicality, they are very case specific and their results cannot be generalized easily as things could change suddenly, for instance, assuming a different arrangement of the ventilation grilles or a different relative position between an infected and a susceptible individual. Some other work remain more general using CFD to focus on the exhalations from an isolated individual in a quiescent environment. In Ref. 5, the effect of head motion and pressure variation at the mouth during a sneeze is discussed finding how the exhaled breath cloud is mostly tilted upward favoring the droplet dispersion over larger distances. In Ref. 6, instead, the role of ambient relative humidity on the evaporation of droplet from a sneeze is analyzed. The effectiveness of face masks in absorbing the larger droplets and limiting the diffusion of smaller droplets is assessed numerically in Refs. 7 and 8, and experimentally in Ref. 9.

Leaving the CFD behind, other works in the literature tackle the problem using cheaper simulation means such as codes for the dynamic modeling of the air quality indices in buildings. In Ref. 10, a Monte Carlo method is used to predict the risk of contagion in a classroom for different ventilation control strategies, while in Ref. 11, multi-objective optimization has been applied in a similar indoor environment to find trade-off solutions between energy consumption and risk of infection.

Another less computationally intensive approach found in the literature regards the creation of models where the governing equations can be solved analytically on a droplet-to-droplet basis and evaluted numerically to better address the varying boundary conditions seen by the droplet during its flight. Important aspects of these models are those already mentioned above: the evaluation of the droplet transport and evaporation, the modeling of the breath cloud, and the role of turbulent dispersion. In Ref. 12, the breath cloud is modeled as a steady non-buoyant jet while turbulent dispersion is not accounted for. The focus of the analysis is on the role of relative humidity on droplet evaporation. Similar modeling assumptions are found in Ref. 13, where a multiple shell model is proposed to account for temperature and concentration gradients inside the droplet. This allows for better predictions of the final stage of the evaporation process. In Refs. 14 and 15, the breath cloud buoyancy is added to the model through the use of empirical formulas for steady jets first proposed in Ref. 16, while the breath cloud model is further expanded by including the role of the jet potential core and assuming a self-similar non-uniform air velocity profile in the jet. In Refs. 17 and 18, turbulent dispersion is modeled with a discrete random walk approach where the air velocity fluctuations in the breath cloud are stochastic functions of the turbulent kinetic energy and of the turbulent dissipation rate. Spatial fields for these quantities are thus needed, and are usually taken from empirical formulas for steady jets found in the literature.[19] The introduction of the random walk model allows stochastic analyses of the droplet spatial distribution to be performed. Only recently the steady-state jet hypothesis was abandoned considering that respiratory events are composed of a jet phase where momentum is injected in the domain followed by a puff phase once the exhalation terminates, and these two phases have a different space vs time evolution. This was investigated experimentally in Ref. 20 and translated into a numerical model in Ref. 21 starting from momentum conservation hypothesis under the assumptions of steady jet phase and uniform spatial velocity in the cloud.

In a recent work by the authors,[22] the breath cloud model was further extended to address any type of unsteady and intermittent velocity input at the mouth, being thus able to render also periodic respiratory events such as breathing, and any type of inlet velocity profile, given that the profile is assumed self-similar across the expanding breath cloud in space. Although the analysis stems from momentum conservation considerations, momentum dissipation in the cloud is modeled with the introduction of a momentum decay characteristic time. Finally, the droplet ejection is randomized in time, within the time span of the exhalation jet phase, and in space, within the mouth/nose cross section, thus adding to the statistical relevance of the stochastic analyses that can be performed with such a model. The randomization in time becomes significant as the breath cloud is no longer modeled as a steady jet.

While fluid mechanics can provide useful information on the droplet trajectory dispersion, which is a quantity certainly correlated with the risk of disease transmission, this is not enough to complete the picture. Additional elements are needed for a tentative quantification.

First of all, an estimate of the exhaled droplet number and size distribution is required. A relatively large number of papers addressed the issue focusing on different types of respiratory events since the pioneering work of Duguid.[23] To cite a few: speaking and coughing are analyzed in Ref. 24, speaking, whispering, mouth breathing, and nose breathing in Ref. 25, breathing, speaking, and singing in Ref. 26. Droplet sizes from a fraction of micrometer up to a millimeter are found, depending on the type of respiratory event, but on their quantity and distribution there is no agreement in the literature. A limit may reside in the experimental methods and in the instruments employed not being able to capture the size correctly over such a large range of scales. In Ref. 27, many of these studies are compared finding that the results can be reasonably overlapped if properly normalized. This leads to the assumption of a power-law distribution of exponent 2 as best compromise solution for the droplet size in any type of respiratory event.[21]

Second, an estimate of the virus concentration in the saliva is needed to evaluate the potential virus shedding rate. For the case of SARS-CoV-2, an average concentration of 3.3 copies/nl was measured in Ref. 28 even though this value can change significantly as the disease progresses. Values as high as 120 copies/nl were measured in hospitalized patients.[29]

As for the infectious dose likely to cause the disease, it is believed to be around 100 copies,[30] a value similar to that known for influenza. Furthermore, the infectious titer decay of SARS-CoV-2 virus has been measured in 1.1, 5.6, and 6.8 h half-life in air, on stainless steel, and on plastic surfaces, respectively.[31]

Information on the quantity of exhaled droplets and on the concentration of virus in the saliva allows the virion shedding rate from an infected individual to be estimated.[32] Together with knowledge about the titer decay and the fraction of airborne droplets, this allows to estimate the virus accumulation rate in a closed environment,[30] eventually including the diluting effect of ventilation.[33] This is usually done under the assumption of well-mixed indoor air using the Wells-Riley equation.[34] Finally, with information on the infectious dose, and the exposure time and breathing rate of a susceptible individual the risk of infection can be estimated. This is conveniently done introducing the concept of *quantum* generation rate,[35] i.e., normalizing the virus shedding rate by the infectious dose. The well-mixed hypothesis essentially restricts the analysis to the case of airborne transmission, while other transmission routes also exist.

The World Health Organization, in fact, distinguishes between five routes:[36] direct contact with an infected individual, indirect contact or fomite (i.e., contact with an infected surface), direct inhalation (i.e., inhalation of exhaled droplets over short distances), indirect inhalation or airborne (i.e., inhalation of suspended droplet nuclei accumulated in an environment), orofaecal (through infected feces contaminating air, water sources, or food).

In the present work, the analytical model developed by the authors and mentioned above is used to perform a series of statistical analyses on the droplet trajectory distribution for a large number of droplets and different types of respiratory events (namely, mouth breathing, nose breathing, speaking, coughing, and sneezing). These events are typified with given boundary conditions derived from the literature. Considering that no "standard" respiratory event actually exist, a sensitivity analysis[37] on the impact of the various simulation parameters on the droplet trajectories is also presented. Following the simulation campaign, with additional information on the quantity and size of droplets exhaled in a real event, and on the virus concentration in the saliva, a virus content is associated with every simulated droplet. From the analysis of the droplet trajectories and velocity histories, an estimate of the virus spatial concentration in the neighborhood of an infected individual is derived. This allows to build virus concentration maps. By discriminating between the droplets falling to the ground and those remaining airborne, also a map of virus ground accumulation can be given, together with an estimate of the indirect inhalation transmission risk following from Wells-Riley model. By introducing an inhalation model, the spatial concentration map is translated into an inhalation map predicting the viral load inhaled by a susceptible individual as a function of its relative position with respect to the infected exhaler. The inhaled viral load is then associated with the probability of developing the disease. The analytical model is thus exploited to quantify the risk of infection related to the different transmission routes associated with the exhaled droplet trajectories: namely, indirect contact, direct inhalation, and indirect inhalation.

II. ANALYTICAL MODEL

The analytical model is briefly recalled here, for an extensive discussion the reader is referred to the previous work by the authors in Ref. 22. The model includes equations for the droplet transport, evaporation, energy balance, and nonvolatile fraction. An exhalation model including buoyancy and turbulent dispersion effects completes the work providing the velocity and the thermohygrometric boundary conditions as functions of space and time.

A. Droplet transport

The main forces acting on the droplet during its flight are weight ($\mathscr{W}$) and drag ($\mathscr{D}$),

$$\mathscr{W} = \frac{1}{6}(\rho_\mathrm{p} - \rho_\mathrm{m})\pi \mathbf{g} D_\mathrm{p}^3, \tag{1a}$$

$$\mathscr{D} = -\frac{1}{8} C_\mathrm{d} \rho_\mathrm{m} \pi ||\mathbf{u}_\mathrm{r}|| \mathbf{u}_\mathrm{r} D_\mathrm{p}^2, \tag{1b}$$

while other minor forces can be neglected.[38] In Eq. (1), ρ is the density, D is the diameter, $\mathbf{g}$ is the gravitational acceleration vector assumed directed in the negative z direction, and C_d is the drag coefficient. The subscript "p" refers to the droplet, "m" to the humid air mixture, and $\mathbf{u}_\mathrm{r} = \mathbf{u}_\mathrm{p} - \mathbf{u}_\mathrm{m}$ is the relative velocity of the droplet with respect to the local undisturbed humid air flow. From Newton's second law of motion, by integrating the acceleration twice with initial conditions on the relative velocity ($\mathbf{u}_\mathrm{r}(0) = \mathbf{u}_{\mathrm{r},0}$) and position ($\mathbf{s}_\mathrm{p}(0) = \mathbf{s}_{\mathrm{p},0}$),

$$\mathbf{u}_\mathrm{p}(t) = \mathbf{u}_\mathrm{m} + \mathbf{u}_{\mathrm{r},0} \mathrm{e}^{-t/\tau_\mathrm{d}} + \mathbf{u}_{\mathrm{r,t}} \frac{\tau_\mathrm{d}}{\tau_{\mathrm{d,t}}} (1 - \mathrm{e}^{-t/\tau_\mathrm{d}}) \tag{2}$$

and

$$\mathbf{s}_\mathrm{p}(t) = \mathbf{s}_{\mathrm{p},0} + \left(\mathbf{u}_\mathrm{m} + \mathbf{u}_{\mathrm{r,t}} \frac{\tau_\mathrm{d}}{\tau_{\mathrm{d,t}}}\right) t + \left(\mathbf{u}_{\mathrm{r},0} - \mathbf{u}_{\mathrm{r,t}} \frac{\tau_\mathrm{d}}{\tau_{\mathrm{d,t}}}\right) \tau_\mathrm{d} (1 - \mathrm{e}^{-t/\tau_\mathrm{d}}), \tag{3}$$

are found, where τ_d is the drag characteristic time, and the subscript "t" denotes the terminal condition, i.e., the condition attained by the droplet in the limit for time that tends to infinity, when $\dot{\mathbf{u}}_\mathrm{r} = \mathbf{0}$. The analytical expressions of the quantities introduced in Eqs. (2) and (3) are as follows:

$$\tau_\mathrm{d} = \frac{4 \rho_\mathrm{p} D_\mathrm{p}}{3 C_\mathrm{d} \rho_\mathrm{m} ||\mathbf{u}_\mathrm{r}||}, \tag{4a}$$

$$\tau_{\mathrm{d,t}} = \sqrt{\frac{4 \rho_\mathrm{p} D_\mathrm{p}^2}{3 C_{\mathrm{d,t}} (\rho_\mathrm{p} - \rho_\mathrm{m}) \rho_\mathrm{m} ||\mathbf{g}||}}, \tag{4b}$$

$$\mathbf{u}_{\mathrm{r,t}} = \left(1 - \frac{\rho_\mathrm{m}}{\rho_\mathrm{p}}\right) \mathbf{g} \tau_{\mathrm{d,t}}, \tag{4c}$$

where the terminal drag coefficients $C_{\mathrm{d,t}}$ is evaluated at the terminal velocity $\mathbf{u}_{\mathrm{d,t}}$. Recurring to one of the many correlations for the flow past a sphere available in the literature, the drag coefficient can be computed as a function of the Reynolds number, evaluated using $||\mathbf{u}_\mathrm{r}||$ as reference velocity. Due to the small size of the droplets, the Cunningham slip correction factor[39] should be possibly included in the drag coefficient formula. A model for droplet-to-droplet interaction, i.e., collision and coalescence, is not included: droplet concentration in respiratory events, in fact, is anyhow small enough for these interactions to be negligible even close to the mouth.[24]

B. Droplet evaporation

From convection-diffusion equation written in stationary form and without source term, and neglecting cross-diffusion of air in water a relatively simple formula expressing the droplet diameter rate of change due to evaporation can be derived,

$$\dot{D}_\mathrm{p} = -\frac{K}{2D_\mathrm{p}} = -\frac{2D_{\mathrm{v,s}}\mathrm{Sh}}{\rho_\mathrm{p} D_\mathrm{p} R_\mathrm{v} T_\mathrm{p}} \frac{p}{p_{\mathrm{a,s}}} (p_{\mathrm{v,s}} - p_{\mathrm{v},\infty}), \tag{5}$$

where $K = -\mathrm{d}D_\mathrm{p}^2/\mathrm{d}t$ is the evaporation rate, D_v is the binary diffusion coefficient of water in air, Sh is the Sherwood number, R_v is the water vapor specific gas constant, T is temperature, and p is pressure. Subscript "a" refers to dry air, "v" refers to water vapor, "s" refers to the value at the droplet surface, and "∞" refers to the ambient value away from the droplet surface. The Sherwood number can be evaluated using the well-known Ranz–Marshall empirical correlation.[40,41] From the definition of evaporation rate, integrating Eq. (5) with the initial condition $D_\mathrm{p}(0) = D_{\mathrm{p},0}$,

$$D_\mathrm{p}(t) = \sqrt{D_{\mathrm{p},0}^2 - Kt} \tag{6}$$

follows.

C. Droplet energy balance

With regard to thermal energy, the droplet sensible energy rate of change is balanced by convective heating and evaporative cooling. Casting the energy balance in terms of droplet temperature rate of change,

$$\dot{T}_\mathrm{p} = \frac{T_{\mathrm{s,t}} - T_\mathrm{p}}{\tau_\mathrm{e}}, \tag{7}$$

where $T_{\mathrm{s,t}}$ is the droplet terminal temperature and τ_e is the evaporation characteristic time. These quantities are defined as

$$T_{\mathrm{s,t}} = T_\infty - \frac{h_\mathrm{lt}\rho_\mathrm{p} K}{4\lambda_\mathrm{s}\mathrm{Nu}}, \tag{8a}$$

$$\tau_\mathrm{e} = \frac{c_{\mathrm{p,p}}\rho_\mathrm{p} D_\mathrm{p}^2}{6\lambda_\mathrm{s}\mathrm{Nu}}, \tag{8b}$$

where h_lt is the water latent heat of vaporization, λ_s is the air thermal conductivity at the droplet surface, c_p is the water specific heat at constant pressure, and Nu is the Nusselt number that can be evaluated from empirical correlations alike those used for the Sherwood number. Integrating Eq. (7) with initial condition $T_\mathrm{p}(0) = T_{\mathrm{p},0}$, the droplet temperature is written as

$$T_\mathrm{p}(t) = T_{\mathrm{p},0}\mathrm{e}^{-t/\tau_\mathrm{e}} + T_{\mathrm{s,t}}(1 - \mathrm{e}^{-t/\tau_\mathrm{e}}). \tag{9}$$

D. Droplet nonvolatile fraction

If the droplet is assumed as composed of water and a generic nonvolatile solute solid fraction, the droplet thermophysical properties appearing in the equations above can be written as weighted averages of the properties of its parts,

$$\rho_\mathrm{p} = \rho_\mathrm{sl}\varphi_\mathrm{sl} + \rho_\mathrm{lq}\varphi_\mathrm{lq}, \tag{10a}$$

$$c_{\mathrm{p,p}} = c_{\mathrm{p,sl}}\omega_\mathrm{sl} + c_{\mathrm{p,lq}}\omega_\mathrm{lq}, \tag{10b}$$

$$M_\mathrm{p} = M_\mathrm{sl} y_\mathrm{sl} + M_\mathrm{lq} y_\mathrm{lq}, \tag{10c}$$

where M is the molar mass, φ is the volume fraction, ω is the mass fraction, and y is the molar fraction. The subscript "sl" refers to the solid fraction, and "lq" refers to the liquid one, and of course the sum of the two fractions must equal 1. With a few algebraic passages water molar fraction results,

$$y_\mathrm{lq} = \left(1 + \frac{M_\mathrm{lq}}{M_\mathrm{sl}} \frac{\rho_\mathrm{sl}}{\rho_\mathrm{lq}} \frac{\varphi_\mathrm{sl}}{\varphi_\mathrm{lq}}\right)^{-1}, \tag{11}$$

and the solid volume fraction evolution is easily computed as a function of the droplet diameter in time. According to Raoult's law,[42] the presence of the solute reduces the water vapor partial pressure at the droplet surface proportionally to y_lq, and so the evaporation rate is reduced as the droplet evaporates and the solute becomes the dominant phase.

E. Exhalation model

The breath cloud is a warm humid air stream gradually mixing with ambient air by entrainment. As such, its velocity and thermohygrometric properties also change gradually. Within this cloud, respiratory droplets are exhaled. As long as the droplet finds itself within the breath cloud boundaries, an exhalation model is necessary to provide the correct and ever changing ambient conditions to the analytical model outlined above.

The model proposed stems from the theory of uniform steady jets and from momentum conservation hypothesis, and is then expanded to account for non-uniformity, unsteadiness, and momentum dissipation. It is assumed that the breath cloud grows radially from the mouth in the shape of a spherical sector characterized by a constant entrainment coefficient β, so that at a generic distance r the cloud half width is $b = \beta r$. The cloud thermodynamic properties are computed as the result of mixing between the exhaled and the entrained air streams. The jet velocity decreases with the distance from the mouth while the jet mass flow rate grows inversely as

$$\frac{u(\xi)}{u_0} = \frac{1}{\xi}\sqrt{\frac{\rho_0}{\rho(\xi)}} = \frac{\dot{m}_0}{\dot{m}(\xi)}, \tag{12}$$

where the subscript "0" denotes the mouth cross section and $\xi = r\beta/r_\mathrm{mt}$ is the non-dimensional distance from the spherical sector tip normalized against the distance between the mouth cross section and the tip itself, r_mt being the mouth opening radius. In this way, $u_0 = u(1)$ is the velocity at the mouth cross section.

A non-uniform velocity profile in the cloud can be modeled by assuming a self-similar radial profile given by any normalized function of the non-dimensional distance from the jet centerline $\zeta = b/\xi r_\mathrm{mt}$, b being the distance from the jet centerline. For instance, if a bell-shaped Gaussian velocity profile is assumed,

$$\frac{u(\xi,\zeta)}{u_0} = \frac{1}{\xi}\sqrt{\frac{\rho_0}{\rho(\xi)}}\mathrm{e}^{-\zeta^2}, \tag{13}$$

where $u_0 = u(1,0)$ is the centerline velocity at the mouth.

To account for the unsteadiness and the possible periodicity of the air mass flow rate in respiratory events, it is assumed that the velocity field retains the shape in Eq. (13) and, at any time, is uniformly scaled by a factor $\gamma(t)$ derived from momentum conservation hypothesis,

$$\gamma(t) = \frac{\dfrac{P(t)}{\dot{P}_\mathrm{st}}}{\sqrt{2\displaystyle\int_0^t \frac{P(t)}{\dot{P}_\mathrm{st}}\,\mathrm{d}t}}, \tag{14}$$

where $P(t)$ is the cumulative momentum injected since the beginning of the respiratory event,

$$P(t) = \int_0^t \dot{P}(t)\,\mathrm{d}t, \tag{15}$$

and $\dot{P}_{\mathrm{st}}$ the momentum flux injected by a reference steady jet. If this quantity is computed taking the time-average centerline velocity at the mouth $\bar{u}_0 = \bar{u}(1,0)$ as reference, then the velocity field in the cloud becomes

$$\frac{u(\xi,\zeta,t)}{\bar{u}_0} = \frac{1}{\xi}\sqrt{\frac{\rho_0}{\rho(\xi)}}\mathrm{e}^{-\zeta^2}\gamma(t), \tag{16}$$

while for steady jets, $\gamma(t) = 1$.

Equation (16) can be evaluated for any type of unsteady and non-uniform velocity impulse at the mouth. For instance, here the following piecewise sinusoidal breathing function is assumed,

$$\frac{u(1,\zeta,t)}{\bar{u}_0} = \begin{cases} \dfrac{\pi}{2}\mathrm{e}^{-\zeta^2}\sin\left(\dfrac{\pi}{2}\dfrac{t}{t_{\mathrm{pk}}}\right), & 0 \le t < t_{\mathrm{pk}}, \\ \dfrac{\pi}{2}\mathrm{e}^{-\zeta^2}\cos\left(\dfrac{\pi}{2}\dfrac{t-t_{\mathrm{pk}}}{t_{\mathrm{ex}}-t_{\mathrm{pk}}}\right), & t_{\mathrm{pk}} \le t < t_{\mathrm{ex}}, \\ 0, & t_{\mathrm{ex}} \le t < t_{\mathrm{pr}}, \end{cases} \tag{17}$$

where the subscript "pk" denotes the peak velocity, "ex" the end of the exhalation, and "pr" the period in the case of periodic event (if the event is isolated, i.e., non-periodic, then $t_{\mathrm{pr}} = \infty$ is assumed). This function stems from considering how in respiratory events the velocity usually peaks quickly and declines more slowly.[43,44] Figure 1(a) shows the trend in time of the velocity at the mouth over a period according to Eq. (17).

Momentum dissipation in the breathing cloud can be accounted for by adding an exponential decay, function of time, to the momentum flux in Eq. (15),

$$P(\tilde{t}) = \int_0^{\tilde{t}} \dot{P}(t)\mathrm{e}^{-(\tilde{t}-t)/\tau_{\mathrm{ds}}}\,\mathrm{d}t, \tag{18}$$

where τ_{ds} is a characteristic momentum dissipation time.

Breath cloud buoyancy is enforced in the model using an empirical formula taken from the literature on steady jets[16] where the centerline shift in the vertical direction is given as a function of the distance from the mouth. In non-dimensional form this is recasted as

$$\Delta\xi_z = 0.0354\frac{g r_{\mathrm{mt}}}{\bar{u}_0^2\beta^2\sqrt{\pi}}\frac{T_0 - T_\infty}{T_\infty}(\xi-1)^3, \tag{19}$$

where $\Delta\xi_z = \Delta z\beta/r_{\mathrm{mt}}$. As an example, Fig. 1(b) reports the effect of buoyancy on the breath cloud centerline for the case of $r_{\mathrm{mt}} = 1$ cm, $\bar{u}_0 = 1$ m/s, $\beta = 0.1$, $T_\infty = 25$ °C, and $T_0 = 34$ °C. The value of ξ to be used in Eq. (16) is then computed on the curved centerline trajectory.

Last, the jet potential core is modeled by forcing $\xi = 1$ within a certain distance from the mouth, usually taken as $12.4r_{\mathrm{mt}}$,[15] and rescaling ξ accordingly at further distances in Eq. (16).

F. Turbulent dispersion and droplet randomization

Droplet turbulent dispersion is modeled with a discrete random walk approach mimicking the interaction between the droplet and a sequence of turbulent eddies. If turbulence is assumed isotropic, the velocity fluctuation $\mathbf{u}'$ is computed as

$$\mathbf{u}' = \boldsymbol{\eta}\sqrt{\frac{2k}{3}}, \tag{20}$$

where k is the turbulent kinetic energy at the droplet location and $\boldsymbol{\eta}$ is a normally distributed random number vector. This perturbation is to be added to $\mathbf{u}_{\mathrm{m}}$ term in Eqs. (2) and (3) and is updated at interval of times equal to

$$\min\left[0.3\frac{k}{\varepsilon}, -\tau_{\mathrm{d}}\ln\left(1 - \frac{0.164k^{1.5}}{\varepsilon\tau_{\mathrm{d}}||\mathbf{u}_{\mathrm{r}}||}\right)\right], \tag{21}$$

where ε is the turbulent dissipation rate. Empirical formulas for k and ε fields in jets as given in Ref. 45 are used in Eqs. (20) and (21).

The random walk approach allows statistical analyses on the droplet trajectory distribution to be performed. This feature is further

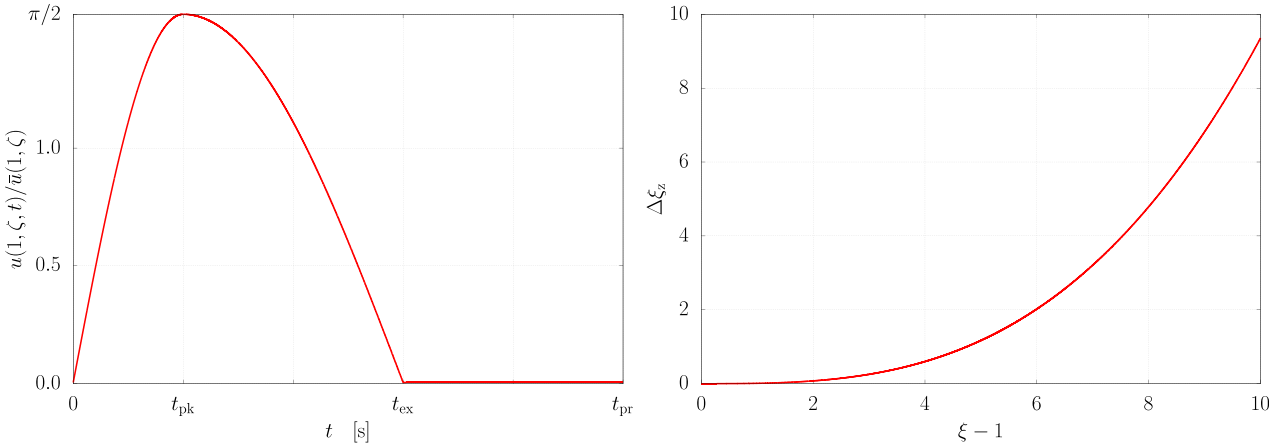

(a) Breathing function according to Eq. (17)

(b) Breath cloud centreline vertical shift due to buoyancy according to Eq. (19)

FIG. 1. Breathing and breath cloud buoyancy functions.

enhanced by considering how a droplet can be exhaled at any point within the mouth cross section and at any time within the exhalation duration, and this affects its trajectory. A randomization of the droplet initial position and time has been implemented where the probability distribution of these two quantities follows the shape of the spatial velocity profile and of the mass flow rate impulse in time, respectively, meaning that a droplet is most likely exhaled where and when the velocity at the mouth is higher. The initial droplet velocity is assumed aligned with the local exhaled flow and having an initial velocity chosen as a given fraction of the local air flow velocity.

G. Inhalation model

To evaluate the chance of inhaling a suspended droplet and assess the risks associated with this, an inhalation model is needed. Here, it is simply assumed that a hemispherical volume V_{in} located in front of the mouth/nose of a breathing susceptible individual is inhaled at each breath. The radius of the inhaled hemisphere is, thus,

$$r_{\text{in}} = \sqrt[3]{\frac{3V_{\text{in}}}{2\pi}}, \tag{22}$$

and if a uniform inhalation over a time span t_{in} and a mouth radius r_0 are further assumed, the inhalation velocity modulus varies with the distance from the mouth as

$$u_{\text{in}}(r) = \frac{V_{\text{in}}}{2\pi t_{\text{in}} \max(r, r_0)^2}, \tag{23}$$

where the max function is introduced to avoid singularities and the velocity vector $\mathbf{u}_{\text{in}}$ is directed radially toward the mouth center. Any droplet crossing the inhaled volume in its trajectory with velocity $\mathbf{u}_{\text{p}}$ is assumed inhaled with a probability $t_{\text{in}}/t_{\text{pr}}$ if its velocity component orthogonal to $\mathbf{u}_{\text{in}}$ is smaller in modulus than $\mathbf{u}_{\text{in}}$ itself, that is to say, if

$$||\mathbf{u}_{\text{p}} - (\mathbf{u}_{\text{p}} \cdot \hat{\mathbf{u}}_{\text{in}})\hat{\mathbf{u}}_{\text{in}}|| < ||\mathbf{u}_{\text{in}}||, \tag{24}$$

where $\hat{\mathbf{u}} = \mathbf{u}/||\mathbf{u}||$ denotes the unit vector. The simple inhalation criteria in Eq. (24) implies that the inertia of the droplets is small enough so that they are quickly deviated by a faster local air stream such as the one that may be induced by inhalation. This is mostly true, in particular for small droplets such as the ones remaining airborne.

The analytical model presented in Sec. II was validated in the previous work from the authors,[22] to which the reader is referred for additional information, against the very sparse literature available. An excellent agreement was found with the experimental works on droplet evaporation.[41,46,47] Droplet transport and the resulting trajectory could be successfully validated against simpler analytical works[14,48] based on the emission of isolated droplets with no turbulent dispersion. To the author knowledge, in fact, no experimental work on this topic exists in the literature. The turbulent dispersion model implemented, instead, is based on a simple and classical approach widely accepted in the numerical community.

III. EXHALATION DATA

In addition to the analytical model summarized above, further information is needed to quantify the potential risk of an infectious disease transmission. This regards the exhaled droplet size distribution and quantity, the virus concentration in the saliva, the infectious dose, and the virus titer decay.

Concerning the exhaled droplet size distribution, as mentioned, there is not much agreement in the literature. A power-law Probability Density Function (PDF) $\mathscr{B}$ is assumed here, in line with,[21] as best compromise solution for all respiratory events,

$$\mathscr{B}(D_{\text{p}}) = \frac{B}{D_{\text{p}}^m}, \tag{25}$$

where B and m are constants to be determined. Similarly, in the literature, it is speculated that virus concentration may not be uniform since droplets of different size could be generated in different sections. of the airways and smaller droplets might be characterized by a higher concentration of virus.[49,50] The evidence of this, however, is still vague. Most likely, smaller droplets are more infectious since they are able to penetrate the lower airways and reach the lungs more easily.[51] In either case, the global effect would be that of increasing the relative danger associated with smaller droplets, and this can be modeled by assuming a power-law PDF $\mathscr{I}$ for the infectious dose,

$$\mathscr{I}(D_{\text{p}}) = ID_{\text{p}}^n, \tag{26}$$

where I and n are constants to be determined. By integrating Eq. (25) over a generic range of diameters $[D_{\min}, D_{\max}]$ associated with a respiratory event, several quantities of interest can be computed, such as, the total number of exhaled droplets,

$$N_{\text{D}} = \int_{D_{\min}}^{D_{\max}} \frac{B}{D_{\text{p}}^m}\, \mathrm{d}D_{\text{p}} = \begin{cases} B\dfrac{D_{\max}^{1-m} - D_{\min}^{1-m}}{1-m} & \text{for } m \neq 1, \\ B\ln\left(\dfrac{D_{\max}}{D_{\min}}\right) & \text{for } m = 1, \end{cases} \tag{27}$$

their overall volume,

$$V_{\text{D}} = \int_{D_{\min}}^{D_{\max}} \frac{B}{D_{\text{p}}^m}\frac{\pi D_{\text{p}}^3}{6}\, \mathrm{d}D_{\text{p}} = \begin{cases} \dfrac{\pi B}{6}\dfrac{D_{\max}^{4-m} - D_{\min}^{4-m}}{4-m} & \text{for } m \neq 4, \\ \dfrac{\pi B}{6}\ln\left(\dfrac{D_{\max}}{D_{\min}}\right) & \text{for } m = 4, \end{cases} \tag{28}$$

and the number of virus exhaled,

$$N_{\text{V}} = c_{\text{sv}} V_{\text{D}}, \tag{29}$$

where c_{sv} is the virus concentration in the saliva, assumed uniform. From Eq. (28), the constant B can be determined as a function of the total exhaled volume V_{D}. The number of quanta emitted becomes

$$\begin{aligned} Q_{\text{D}} &= \int_{D_{\min}}^{D_{\max}} \frac{B}{D_{\text{p}}^m}\frac{\pi D_{\text{p}}^3}{6}\frac{c_{\text{sv}}}{ID_{\text{p}}^n}\, \mathrm{d}D_{\text{p}} \\ &= \begin{cases} \dfrac{\pi B c_{\text{sv}}}{6I}\dfrac{D_{\max}^{4-m-n} - D_{\min}^{4-m-n}}{4-m-n} & \text{for } m+n \neq 4, \\ \dfrac{\pi B c_{\text{sv}}}{6I}\ln\left(\dfrac{D_{\max}}{D_{\min}}\right) & \text{for } m+n = 4. \end{cases} \end{aligned} \tag{30}$$

Considering that the average infectious dose is $\bar{I} = N_{\text{V}}/Q_{\text{D}}$, the constant I can be evaluated as

TABLE I. Estimate of the B coefficient for the different respiratory events.

Type of event	Exhaled air volume	Period	Range of diameters	B
Breathing	600 cm^3	4 s	$[10^{-1}, 10^{+1}]$ μm	3.0×10^{-5} m
Speaking	600 cm^3	4 s	$[10^{-1}, 10^{+2}]$ μm	6.0×10^{-5} m
Coughing	1000 cm^3		$[10^{-1}, 10^{+3}]$ μm	2.0×10^{-2} m
Sneezing	2000 cm^3		$[10^{-1}, 10^{+3}]$ μm	2.0×10^{-1} m

$$I = \begin{cases} \bar{I} & \text{for } n = 0, \\ -\dfrac{\bar{I}}{n} \dfrac{D_{\max}^{-n} - D_{\min}^{-n}}{\ln (D_{\max}/D_{\min})} & \text{for } n \neq 0,\ m = 4, \\ \bar{I} n \dfrac{\ln (D_{\max}/D_{\min})}{D_{\max}^{n} - D_{\min}^{n}} & \text{for } n \neq 0, m + n = 4, \\ \bar{I} \dfrac{4 - m}{4 - m - n} \dfrac{D_{\max}^{4-m-n} - D_{\min}^{4-m-n}}{D_{\max}^{4-m} - D_{\min}^{4-m}} & \text{otherwise.} \end{cases} \tag{31}$$

In the case of a periodic respiratory event, Eqs. (27)–(30) can be divided by the period to provide the respective rates.

In the following, $m = 2$ is chosen as suggested in, Ref. 21, and $n = 1$ is arbitrary assumed due to the lack of clear quantitative information in the literature. This choice enhances the virus airborne fraction in the results that follow so that predictions of the inhalation risk are likely in favor of safety. The virus concentration in the saliva is set to $c_{sv} = 3.3$ copies/nl, this being the average concentration found in Ref. 28 for SARS-CoV-2, while the average infectious dose $\bar{I} = 100$ copies/quantum is assumed following Ref. 30. By definition, the average infectious dose represents the number of inhaled viruses sufficient to induce the disease with a probability of $1 - e^{-1} = 63\%$ in a susceptible individual. Considering that droplet size in the range from 0.1 μm to 1 mm have been reported for respiratory events,[27] from Eq. (31) $I = 199\ 980$ copies/(quanta · m) follows. The value of the constant B, instead, depends on the type of respiratory event. In Ref. 27, a review on the range of droplets size and concentration measured in several works for breathing, speaking, coughing, and sneezing is presented. Despite the results of the various works compared may even differ by orders of magnitude, by averaging the results logarithmically and assuming the exhaled air volume associated with each respiratory event, the coefficient B can be estimated using Eq. (27). The result of this operation is resumed in Table I. Data in the table are to be intended per respiratory event. For breathing and speaking, an exhaled flow of 9 l/min is assumed with breathing period of 4 s,[44] while for coughing and sneezing exhaled volumes of 1 and 2 l are assumed, respectively.[43] The large range mentioned above for the droplet size holds for coughing and sneezing, while during milder respiratory events such as breathing and speaking larger droplets are not expelled. An upper threshold of 10 μm for breathing, and 100 μm for speaking is chosen in the current work in line with some previous study.[27,52]

Table II resumes the results of Eqs. (27)–(30) given the assumptions above. The results are reported for the different respiratory events and are split by droplet size order of magnitude. In the case of periodic event hourly rates are given, while for coughing and sneezing, data are to be intended per event. It can be seen how moving from one order of magnitude to the next the number of droplets is reduced by a factor of 10, the overall droplet volume grows by a factor of 100, and the number of quanta emitted increases by a factor of 10. This follows from the values chosen for m and n coefficients. By considering that in standard temperature and relative humidity conditions the critical diameter (i.e., the diameter below which a droplet remains airborne) is slightly smaller than 100 μm, it can be deduced that with this choice in the case of coughing and sneezing the airborne fraction includes $\approx 99.9\%$

TABLE II. Droplet number and cumulative volume, virus number and quanta distribution associated with different respiratory events.

Type of event	Range of diameters	Droplet number (N_D)	Droplet cumulative volume (V_D)	Virus number (N_V)	Number of quanta (Q_D)
Breathing	$[10^{-1}, 10^{+0}]$ μm	$2.43 \times 10^{+5}$/h	7.00×10^{-6} mm^3/h	2.31×10^{-2}/h	2.10×10^{-1}/h
	$[10^{+0}, 10^{+1}]$ μm	$2.43 \times 10^{+4}$/h	7.00×10^{-4} mm^3/h	$2.31 \times 10^{+0}$/h	$2.10 \times 10^{+0}$/h
	Total	$2.67 \times 10^{+5}$/h	7.07×10^{-4} mm^3/h	$2.33 \times 10^{+0}$/h	$2.31 \times 10^{+0}$/h
Speaking	$[10^{-1}, 10^{+0}]$ μm	$4.86 \times 10^{+5}$/h	1.40×10^{-5} mm^3/h	4.62×10^{-2}/h	4.20×10^{-1}/h
	$[10^{+0}, 10^{+1}]$ μm	$4.86 \times 10^{+4}$/h	1.40×10^{-3} mm^3/h	$4.62 \times 10^{+0}$/h	$4.20 \times 10^{+0}$/h
	$[10^{+1}, 10^{+2}]$ μm	$4.86 \times 10^{+3}$/h	1.40×10^{-1} mm^3/h	$4.62 \times 10^{+2}$/h	$4.20 \times 10^{+1}$/h
	Total	$5.39 \times 10^{+5}$/h	1.41×10^{-1} mm^3/h	$4.66 \times 10^{+2}$/h	$4.66 \times 10^{+1}$/h
Coughing	$[10^{-1}, 10^{+0}]$ μm	$1.80 \times 10^{+5}$	5.18×10^{-6} mm^3	1.71×10^{-2}	1.56×10^{-1}
	$[10^{+0}, 10^{+1}]$ μm	$1.80 \times 10^{+4}$	5.18×10^{-4} mm^3	$1.71 \times 10^{+0}$	$1.56 \times 10^{+0}$
	$[10^{+1}, 10^{+2}]$ μm	$1.80 \times 10^{+3}$	5.18×10^{-2} mm^3	$1.71 \times 10^{+2}$	$1.56 \times 10^{+1}$
	$[10^{+2}, 10^{+3}]$ μm	$1.80 \times 10^{+2}$	$5.18 \times 10^{+0}$ mm^3	$1.71 \times 10^{+4}$	$1.56 \times 10^{+2}$
	Total	$2.00 \times 10^{+5}$	$5.24 \times 10^{+0}$ mm^3	$1.73 \times 10^{+4}$	$1.73 \times 10^{+2}$
Sneezing	$[10^{-1}, 10^{+0}]$ μm	$1.80 \times 10^{+6}$	5.18×10^{-5} mm^3	1.71×10^{-1}	$1.56 \times 10^{+0}$
	$[10^{+0}, 10^{+1}]$ μm	$1.80 \times 10^{+5}$	5.18×10^{-3} mm^3	$1.71 \times 10^{+1}$	$1.56 \times 10^{+1}$
	$[10^{+1}, 10^{+2}]$ μm	$1.80 \times 10^{+4}$	5.18×10^{-1} mm^3	$1.71 \times 10^{+3}$	$1.56 \times 10^{+2}$
	$[10^{+2}, 10^{+3}]$ μm	$1.80 \times 10^{+3}$	$5.18 \times 10^{+1}$ mm^3	$1.71 \times 10^{+5}$	$1.56 \times 10^{+3}$
	Total	$2.00 \times 10^{+6}$	$5.24 \times 10^{+1}$ mm^3	$1.73 \times 10^{+5}$	$1.73 \times 10^{+3}$

TABLE III. Synoptic table of the simulation setup.

Ambient	
Pressure	1 atm
Temperature	20 °C
Relative humidity	50%
Air velocity	0 and 0.05 m/s
Air direction	horizontal
Breath	
Temperature	34 °C
Relative humidity	95%
Entrainment coefficient	0.11
Droplet	
Initial temperature	34 °C
Mouth/nose height	1.5 m
Initial velocity and direction	Aligned with and equal to the local breath velocity
Initial solid volume fraction	1%
Solid fraction density	1200 kg/m^3
Solid fraction specific heat	1100 J/kg K
Solid fraction molar mass	0.1 kg/mol

of the droplets exhaled, summing up to ≈ 1% of the overall droplet volume, and ≈ 10% of the quanta emitted. The values of the total liquid volume exhaled reported in the table are in line with those given in mass and mentioned in Ref. 53 for coughing (6.7 mg) and in Ref. 3 for sneezing (50 mg) events.

IV. SIMULATION SETUP

The analytical model outlined in Sec. II has been used to perform statistical analyses of the exhaled droplet trajectory distribution for the cases of mouth breathing, nose breathing, speaking, coughing, and sneezing. The simulation setup for what concerns the ambient, the droplet initial conditions and chemical composition, and the common breath cloud features is fixed and the modeling choices are resumed in Table III. Normal temperature and pressure conditions with 50% relative humidity are assumed. Two ventilation schemes are modeled: one with no ventilation and quiescent ambient air, the other with an average air velocity of 5 cm/s blowing from behind on the infected individual. The breath cloud is assumed at 34 °C and 95% relative humidity, while the entrainment coefficient has been shown in the literature to be ≈ 0.11 for any respiratory event.[43,44] Exhaled droplets are assumed to be released from 1.5 m height, being in thermal equilibrium with the breath cloud, and being composed of a 1% volume solid fraction made of salts and proteins.

Additional boundary conditions are needed to define the breath cloud behavior and these obviously depend on the type of respiratory event to be modeled. Their value is resumed in Table IV. In the literature, there is a limited agreement on the outflow velocities associated with different respiratory events, and it is rarely specified whether the values reported are peak or average ones. The values in Table IV derive from an attempt to critically analyze and average all these data. For breathing, for instance, a value of 1.3 m/s is reported in Ref. 54, while values between 0.5 and 5 m/s are found in Ref. 49 for light to heavy breathing. For coughing 10 m/s peak velocity is reported in Ref. 55, while ≈ 12 m/s average velocity in Ref. 15, with peaks of 22 m/s mentioned in Ref. 53. For sneezing, most common values are between 30 (Ref. 56) and 50 m/s for the peak velocity,[55] whereas a peak volume flow rate of 6 l/s is given in Ref. 57. Time durations of ≈ 0.4–0.5 s are reported for coughing and sneezing[43,55] with peak velocities found after ≈ 0.1 s from the beginning of the exhalation. For breathing, 15 cycles per minute are usually assumed,[58] with the velocity peaking at ≈ 0.8 s.[44] Mouth and nose diameters in Table IV are derived to match the exhaled air volume and the event time span with the average velocity expected. Since, in the present work, the breathing function in Eq. (17) is assumed, $u_{pk}/u_{avg} = \pi/2$ is always attained.

According to Refs. 49 and 59, the direction of the exhaled breath is slightly tilted downward in the case of mouth breathing, while the angle with respect to the horizontal for nose breathing is ≈ 60° (Refs. 44 and 60) and the streams coming from the nostrils are ≈ 20° apart. A cough is usually directed downward by ≈ 27.5°,[43] while during sneezing the direction of the exhalation changes in time due to the head motion,[5] but on average is directed upward by ≈ 27.5°. The breath cloud momentum dissipation characteristic time τ_{ds} is set to 0.8 s for breathing and speaking, 1.0 s for coughing, and 0.3 s for sneezing: from preliminary CFD analyses of an exhaling individual in an empty room these appear to be reasonable choices providing a good match with regard to the extents of the breath cloud in time and space for the different respiratory events.

Although the rationale behind the modeling choices resumed in the tables and presented so far is rather reasonable, it must be

TABLE IV. Synoptic table of the boundary conditions used for modeling the breath cloud for the different respiratory events.

Type of event	Opening diameter (D_{mt})	Breath direction (θ)	Exhaled air volume (V_{ex})	Breathing function times (t_{pk}, t_{ex}, t_{pr})	Opening cross section	Avg. volume flow rate ($\dot{V}_{avg}$)	Average and peak velocity (u_{avg}, u_{pk})	Dissipation time (τ_{ds})
Mouth breathing	16 mm	−5°	600 cm^3	0.8, 2.4, 4.0 s	202 mm^2	250 cm^3/s	1.24, 1.95 m/s	0.8 s
Nose breathing[a]	9 mm	−60°	300 cm^3	0.8, 2.4, 4.0 s	64 mm^2	125 cm^3/s	1.96, 3.08 m/s	0.8 s
Speaking	16 mm	−5°	600 cm^3	0.8, 2.4, 4.0 s	202 mm^2	250 cm^3/s	1.24, 1.95 m/s	0.8 s
Coughing	22 mm	−27.5°	1000 cm^3	0.1, 0.4, ∞ s	381 mm^2	2500 cm^3/s	6.56, 10.30 m/s	1.0 s
Sneezing	18 mm	+27.5°	2000 cm^3	0.1, 0.4, ∞ s	255 mm^2	5000 cm^3/s	19.59, 30.77 m/s	0.3 s

[a]Data per nostril, the two streams are separated by 20° circumferentially on the horizontal.

highlighted that most of these data are subject to large margins of uncertainty for a number of reasons ranging from the difficulties in carrying out accurate measurements, to the lack of experimental data in the literature, to their inherent variability with respect to many factors. More simply, a *standard* breath, cough, or sneeze is just an abstraction that yet is needed to quantitatively try to investigate different scenarios in terms of infectious disease transmission risk.

Two simulation campaigns are carried out for each of the five scenarios in Table IV: one without ventilation, the other with a uniform horizontal ventilation as mentioned above. A set of 972 logarithmically distributed droplet diameter ranges $[D_{\min}, D_{\max}]$ covering the four orders of magnitude from 0.1 μm to 1 mm is modeled and the logarithmic mean diameter D_p in each range simulated so that

$$\frac{D_{\max}}{D_p} = \frac{D_p}{D_{\min}} = 10^{4(0.5/972)} = 1.004\,75. \tag{32}$$

Simulations are repeated $N = 21$ times for each diameter, thus resulting in over 20 000 runs for each campaign. The number of droplet diameters simulated is chosen so that the relative difference in size between adjacent values is $< 1\%$. The post-processing of the results will then skip larger diameters in breathing and speaking events according to the expected ranges defined in Table I. The computational time required by each campaign is ≈ 10 days running in single core on an old workstation equipped with Intel i7-2600 CPU at 3.4 GHz. The time required by the single run varies largely with the droplet size, and goes from a fraction of a second for larger droplets up to ≈ 1.5 min for smaller ones. From each run, a large set of information is collected at each time step, including time, droplet position, velocity, diameter, and temperature, local air velocity, temperature, and relative humidity.

V. POST-PROCESSING

A quanta load Q_D is associated with each of the 972 diameter ranges in the same way as shown in Table II for wider ranges, and to each simulated droplet a load $Q_{D,i} = Q_D/N$ is assigned. In this way, the viral distribution in each simulation campaign is modeled coherently whatever the size distribution and number of simulated droplets. It is therefore sufficient that the number of runs is large enough for the trajectory distribution to be statistically relevant and cover the space in a sufficiently uniformly way.

If a periodic respiratory event is modeled, the virus exhalation may be assumed continuous on average. A certain quanta flow rate $\dot{Q}_{D,i} = Q_{D,i}/t_{pr}$ is associated with each droplet exhaled by the infected individual and a steady quanta concentration is attained in his neighborhood. The average quanta concentration in a generic volume V_c is given by

$$c_c = \sum_i \frac{\dot{Q}_{D,i}}{V_c} t_i = \sum_i \frac{Q_D}{N} \frac{t_i}{t_{pr}} \frac{1}{V_c}, \tag{33}$$

where the sum is made on all the droplets i crossing the volume in their trajectory, t_i is the droplet residence time inside the chosen volume, and c_c is measured in quanta/m^3. The subscript "c" indicates that the concentration is evaluated on a generic volume cell.

In the case of isolated event, no steady concentration is attained. A similar risk measure, named *viral exposure* in Ref. 61 and evaluated in quanta $\cdot$ s/m^3 is obtained if the event period term in Eq. (33) is dropped,

$$e_c = \sum_i \frac{Q_{D,i}}{V_c} t_i = \sum_i \frac{Q_D}{N} \frac{t_i}{V_c}. \tag{34}$$

Equations (33) and (34), deriving from droplet trajectories, are associated with direct inhalation transmission risk.

Multiplying Eq. (33) by the volume V_{in} inhaled by a susceptible individual over the lapse of exposure time,

$$i_c = c_c V_{in} = \sum_i \frac{Q_D}{N} \frac{t_i}{t_{pr}} \frac{V_{in}}{V_c}, \tag{35}$$

or Eq. (34) by the average inhalation flow rate $\dot{V}_{in}$ over the breathing period,

$$i_c = e_c \dot{V}_{in} = \sum_i \frac{Q_D}{N} \frac{\dot{V}_{in}}{V_c} t_i, \tag{36}$$

the number of inhaled quanta i_c is computed as a function of the relative position between infected and susceptible individuals. The sum, this time, must not be made on the droplets intercepting the arbitrary volume V_c along their path but on all the droplets that, passing through the volume inhaled by the susceptible individual, comply with the inhalation condition outlined in Sec. II G. The use of the average inhalation volume flow rate over the breathing period in Eq. (36) allows to statistically account for the chance that when invested by the droplets exhaled during an isolated event, a susceptible individual breathing normally may either inhale them or not depending on the phase of his own breathing cycle.

Once i_c is known, from the definition of *quantum*, the risk for a susceptible individual of contracting an infectious disease when exposed to such exhalations can be quantified as

$$r_c = 1 - e^{-i_c}. \tag{37}$$

In a similar fashion, the quanta concentration per unit area due to droplet deposition on a generic surface S_c following an isolated respiratory event can be computed as

$$c_c = \sum_i \frac{Q_{D,i}}{S_c} = \sum_i \frac{Q_D}{N} \frac{1}{S_c}, \tag{38}$$

where the sum is made on all the droplets i deposited on the surface, and c_c is measured in quanta/m^2. The average deposition rate d_c, in the case of periodic event, is simply found dividing Eq. (38) by the event period,

$$d_c = \sum_i \frac{Q_{D,i}}{S_c} \frac{1}{t_{pr}} = \sum_i \frac{Q_D}{N} \frac{1}{S_c t_{pr}}. \tag{39}$$

Equations (38) and (39) are associated with fomite transmission risk, in the event that the infected surface is touched and its viral load brought in contact with the airways of a susceptible individual.

Multplying Eq. (38) by the surface area touched,

$$i_c = c_c S_c = \sum_i \frac{Q_D}{N}, \tag{40}$$

or Eq. (39) by the surface area touched and by the lapse of time the surface has been exposed to infection t_{ep},

$$i_c = d_c S_c t_{ex} = \sum_i \frac{Q_D}{N} \frac{t_{ep}}{t_{pr}}, \tag{41}$$

the number of inhaled quanta i_c is computed, where the sum is made on all the droplets deposited on the surface and where the ratio t_{ep}/t_{pr} simply denotes the number of periods the surface has been exposed to infection before being touched. In Eqs. (40) and (41), a multiplicative term representing the efficiency with whom the viral load is transferred from the infected surface to the airways through touching could be included. In favor of safety, this term is omitted in the current analysis. Once i_c is known, the risk of infection can still be evaluated using Eq. (37).

From the analysis carried out so far, an estimate of the risk associated with airborne transmission route is still missing. To do this, Wells–Riley equation[34] is used. Let us consider a periodic respiratory event emitting on average $\dot{Q}_D = \dot{Q}_{ab} + \dot{Q}_{gr}$ quanta per second, where the subscripts "ab" and "gr" stand for the airborne fraction and for the fraction deposited on the ground, respectively. Let the characteristic time of the virus removal rate in the room be τ_{rm}, then the quanta accumulation in a confined space can be written in terms of concentration gradient in time under the assumption of well-mixed environment as

$$\frac{dc_{rm}}{dt} = \frac{\dot{Q}_{ab}}{V_{rm}} - \frac{c_{rm}(t)}{\tau_{rm}}, \tag{42}$$

where c_{rm} is expressed in quanta per cubic meter and V_{rm} is the volume of the room. By integrating Eq. (42),

$$c_{rm}(t) = \frac{\dot{Q}_{ab}\tau_{rm}}{V_{rm}}\left(1 - e^{-t/\tau_{rm}}\right) \tag{43}$$

is found, where the characteristic time τ_{rm} follows from the virus titer decay and other factors contributing to virus removal in the room, such as the dilution due to ventilation. If the titer decay is expressed in virus half-life t_{hl} in air, and t_{ac} is the time needed for a complete air change in the room,

$$\frac{1}{\tau_{rm}} = \left(\frac{1}{t_{hl}} + \frac{1}{t_{ac}}\right) \ln 2. \tag{44}$$

For large times t, the virus concentration in the room tends to $\dot{Q}_{ab}\tau_{rm}/V_{rm}$, while the integral average concentration an individual would be exposed to over a given time span, e.g., $[0,\ t_1]$, can be computed by further integration of Eq. (43),

$$\bar{c}_{rm}(t_1) = \frac{\dot{Q}_{ab}\tau_{rm}}{V_{rm}}\left[1 - \frac{\tau_{rm}}{t_1}\left(1 - e^{-t_1/\tau_{rm}}\right)\right]. \tag{45}$$

In the case of isolated respiratory event, a certain amount of airborne quanta Q_{ab} is released at time zero and the initial airborne concentration gradually fades according to its characteristic time, by integrating Eq. (42) without the source term,

$$c_{rm}(t) = \frac{Q_{ab}}{V_{rm}} e^{-t/\tau_{rm}} \tag{46}$$

is found, while the integral average concentration over a time span $[0,\ t_1]$ is given by

$$\bar{c}_{rm}(t_1) = \frac{Q_{ab}}{V_{rm}} \frac{\tau_{rm}}{t_1}\left(1 - e^{-t_1/\tau_{rm}}\right). \tag{47}$$

The same Eqs. (42)–(47) hold also for estimating the concentration on the ground, expressed in quanta/m^2, given that the airborne quanta term is substituted by the amount deposited on the ground, the room volume is substituted by the surface area, and the characteristic time is computed omitting the ventilation term. To be mentioned that virus half-life t_{hl} on the ground depends on the surface type and its value is generally much higher than that found in air. Further, it must be considered that quanta deposition on the ground is not uniform, i.e., the well-mixed hypothesis technically does not hold. Nonetheless, the equations can still be applied to small surfaces whose concentration may well be assumed locally uniform: in this case the terms $\dot{Q}/S$ and Q/S must be intended as local viral deposition rate and local initial concentration, respectively.

In view of airborne infection risk assessment, the average volumetric concentrations over the time span of interest for periodic [Eq. (45)] and isolated [Eq. (47)] respiratory events must be multiplied by the volume inhaled [Eq. (35)] and the result fed into Eq. (37) to compute the quanta inhaled by a susceptible individual and the associated risk of infection, respectively. In virtue of the well-mixed hypothesis, the result of this operation consists in a uniform concentration or in a certain amount of inhaled quanta to be added to the quantities already computed for the direct inhalation transmission route.

With regard to fomite infection risk assessment, instead, the instantaneous spatial concentrations for periodic [Eq. (43)] and isolated [Eq. (46)] respiratory events, actually retrace Eqs. (39) and (38) enriching them with time-dependent terms that allow to address the role of virus titer decay on the surface concentration.

In the simulations performed, the droplet trajectory is tracked up to when the droplet reaches the ground or, in the case of airborne particles, up to when evaporation terminates, thermal equilibrium with the environment is reached, and a terminal velocity below a given threshold of 2 cm/s is attained outside the area of influence of the breath cloud. When this occurs, it is assumed that the airborne droplet nuclei will be transported by the smallest air current, and in the long run will spread uniformly in the room. Information on the droplet trajectory is used to compute the viral inhalation associated with direct inhalation transmission route, information on the droplet deposition is used to evaluate the potential viral inhalation associated with fomite transmission route, and information on the airborne droplets is used to quantify the viral inhalation associated with airborne transmission route.

In the following, the airborne viral concentration is evaluated for a rather severe scenario of $t = 1$ h exposure starting from a virus free environment at time zero, in an average size ($V_{rm} = 300$ m^3) poorly ventilated (1 air change per hour) office, assuming a virus half-life in air of 1.1 h as found in Ref. 31 for SARS-CoV-2. With these data, the room characteristic time computed with Eq. (44) results of ≈ 45 min. The viral concentration at the ground, instead, is evaluated for the same scenario at time $t = 1$ h, given a virus half-life on the surface of 6.2 h (i.e., $\tau_{gr} \approx 9$ h), which is an intermediate value among those mentioned in Ref. 31 for surfaces.

For post-processing purpose, the space in front of the infected individual is meshed with hexahedral cells of a given size (namely, 4 mm). In each cell quanta concentration or viral exposure associated with direct inhalation, transmission route is computed using Eqs. (33) and (34), thus providing practical viral concentration/exposure spatial maps. By further applying the inhalation model in Sec. II G to each cell

center, similar viral inhalation maps are extracted from Eqs. (35) and (36). From these maps, applying Eq. (37), the risk for a susceptible individual of contracting an infectious disease when exposed to the exhalations from an infected individual can be quantified. The uniform airborne concentration after one hour exposure is then evaluated for the office scenario just mentioned from Eqs. (45) and (47), and its contribution added to the maps. The concentration in Eq. (47) is made dimensionally consistent with the viral exposure in Eq. (34) multiplying it by the exposure time.

For visualization needs, since these maps are three-dimensional, the spatial maps that follow are presented on a vertical x–z plane aligned with the direction of the exhalation where the concentrations in the spanwise direction y are cumulated and averaged over the breath cloud width at the given longitudinal distance from the mouth.

In the same way, the ground in front of the infected individual is meshed with squares of a given size (namely, 4 mm) and the quanta concentration per unit area after exposure computed using Eqs. (43) and (46) on the basis of the droplet deposition data obtained from the simulations.

VI. RESULTS

The results of the simulation campaigns described in Sec. IV, including five types of respiratory event and two room ventilations, are presented in this section. The results are given in terms of droplet trajectories, viral concentration/exposure, inhalation, and risk of infection maps on the x–z vertical plane, and in terms of droplet deposition and viral concentration/deposition rate on the x–y ground plane. Animations of the instantaneous viral concentration in time can be found in the multimedia material available online and associated with the present work.

A sensitivity analysis on the effect of the main simulation parameters on the trajectories of droplet of different size is given in the end. This allows to appreciate how changes in the ambient conditions or in the intensity of the respiratory event may affect the results that, out of necessity, are given for a discrete, although large, number of scenarios.

A. Breathing

From Table II, it is noted that the virus exhalations associated with a breathing infected individual is relatively small and has been estimated in 2.3 quanta/h. The droplets exhaled are small enough (see Table I) to be fully transported by the breath cloud, so that the airborne fraction equals 100%. Following Eq. (45), this results in an average airborne viral concentration in the room of $\approx 2.6 \times 10^{-9}$ quanta/cm^3 after one hour exposure, which translates into a minimum of 1.4×10^{-3} quanta/h inhaled by a susceptible individual breathing normally, and corresponding to a risk of infection of 0.14%. The difference between mouth and nose breathing scenarios is limited to the direction and the velocity of the exhalation as summarized in Table IV.

Figure 2 (Multimedia view) resumes the results obtained for the mouth breathing scenario without room ventilation. Figure 2(a) shows the exhaled droplet trajectories that intertwine and overlap within the breath cloud as a result of turbulent dispersion and the different initial conditions. Note that smaller droplet trajectories are drawn on top of larger droplet ones so that large droplet data are mostly covered due to the large number of trajectories at stake. In this scenario, the droplets are so small that the airborne stopping criteria in the simulations are met almost immediately once the droplet exits from the breath cloud boundaries. This may either occur due to the fading of the breath cloud momentum with the distance or to turbulent dispersion pushing the droplet away from the cloud prematurely. The effect of buoyancy, although marginal, is apparent from the curved trajectories. Applying Eq. (33) to each cell, trajectory information is transformed into the viral concentration map in Fig. 2(b). Of course viral concentration is higher close to the mouth of the infected individual and dilutes with the distance. A non-negligible concentration is perceived within the breath cloud extension up to a distance of ≈ 60 cm even for the seemingly harmless mouth breathing scenario. Applying the inhalation model in Sec. II G to the concentration data, the viral inhalation rate in Fig. 2(c) is found, and further applying Eq. (37) to the inhalation rate the risk map in Fig. 2(d) follows. It is worth mentioning how to read these figures: in Fig. 2(c), for instance, each cell is colored according to the predicted viral inhalation rate a susceptible individual breathing normally would be subject to while staying with his mouth or nose at that particular location in space and finding himself in front of (i.e., aligned along the y direction with) a mouth breathing infected individual. The figure accounts both for direct inhalation and airborne transmission routes for the generic condition mentioned in Sec. V. The viral concentration associated with the latter is identified by the lower scale of the color bar and being orders of magnitude lower than that related to the peaks of the direct inhalation route it does not confound its reading. The same considerations hold for all the three maps in Figs. 2(b)–2(d) and for analogous maps presented in the following. The three maps look similar as they represent further elaborations of the same set of data given by the viral content of the single droplets and their trajectories as resumed in Fig. 2(a). The plume appears thicker in Fig. 2(c) since the inhalation rate, following the model in Sec. II G, is essentially a conditional sum of the concentrations over a ≈ 6 cm radius hemisphere.

Figure 3 (Multimedia view) shows the same set of results for the case of nose breathing. Compared to the previous case, the difference in the results is marginal, if not for the different direction assumed by the trajectories. The results of the ventilated breathing scenarios are omitted for brevity. The marginal impact of ventilation on the breath cloud extension is such that the resulting maps are largely similar to those already shown.

B. Speaking

According to Table IV, the boundary conditions adopted for the breath cloud modeling in speaking and mouth breathing scenarios are the same. This choice was made considering that, on average, the breathing period and the overall volume of air exhaled while speaking are indeed similar to those characterizing breathing. Nonetheless, the continuous movement of the lips while speaking will induce irregular air outflow velocity patterns having sharp peaks on plosive sounds.[58] As these patterns much depend on the type of sounds emitted and cannot be generalized, the choice fell on modeling the average behavior, knowing that in reality droplet dispersion will likely be more pronounced than predicted. The main difference between the mouth breathing and speaking models adopted here is that the latter is characterized by a double coefficient B in the droplet size PDF (see Table I) that translates in double exhalations for a given diameter range. Further, the droplet size range of interest extends up to 100 μm, resulting in a twentyfold quanta exhalation rate of 46.6 quanta/h compared to breathing, as summarized in Table II. While the results relative to droplets up to 10 μm in size are the same already seen for mouth

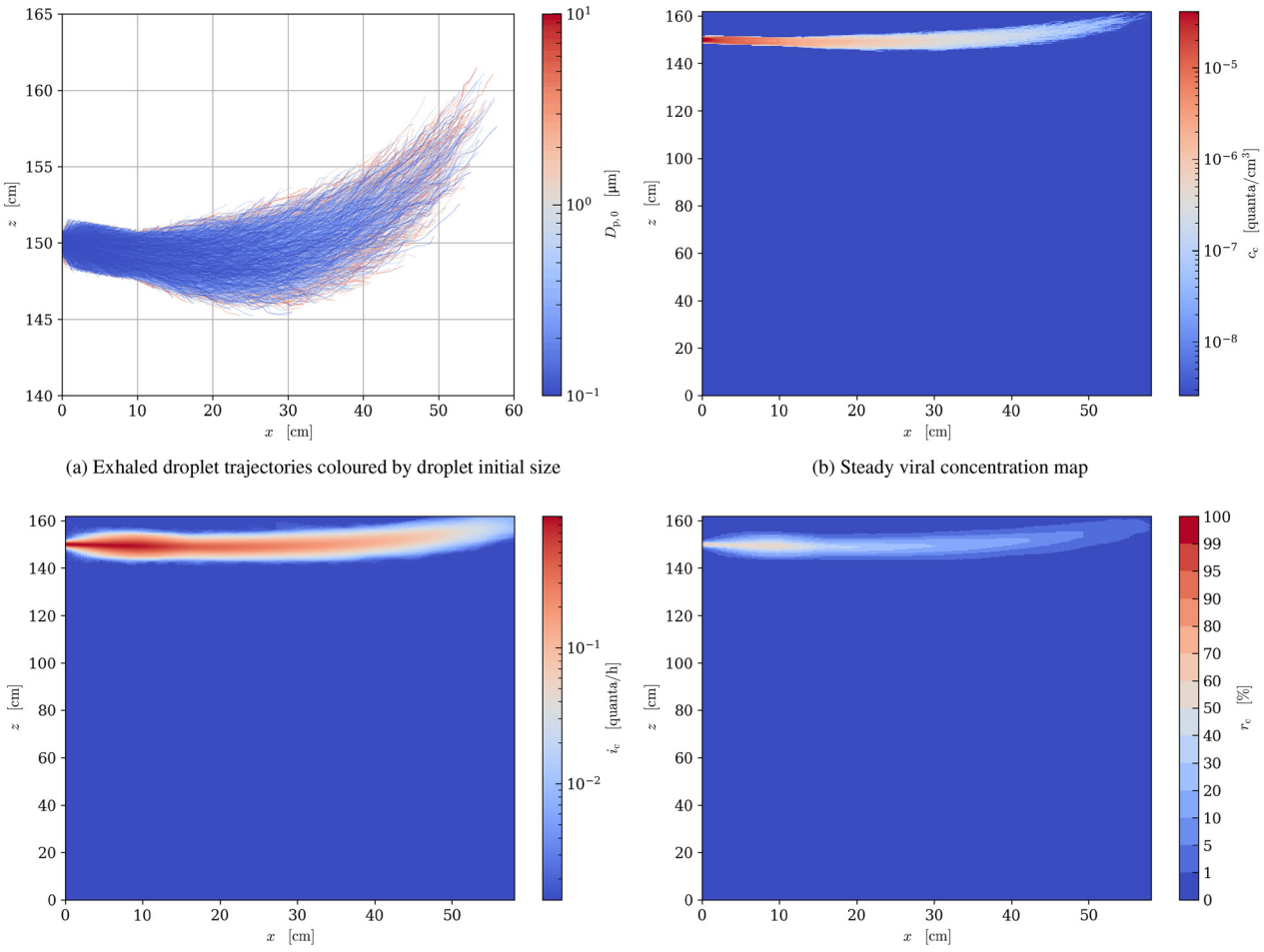

(a) Exhaled droplet trajectories coloured by droplet initial size

(b) Steady viral concentration map

(c) Viral inhalation rate map

(d) Risk of infection map after one hour exposure

FIG. 2. Results of the mouth breathing scenario without room ventilation. Multimedia available online.

breathing scenario, larger droplets are big enough to escape from the breath cloud due to gravity, eventually reaching the ground. After the simulations, a critical diameter of ≈ 91.8 μm is found for both ventilation scenarios, so that the quanta airborne fraction equals 92% of the total (42.8 quanta/h). This translates into an average airborne viral concentration in the room of $\approx 4.8 \times 10^{-8}$ quanta/cm^3 after one hour exposure and a minimum of 2.6×10^{-2} quanta/h inhaled by a susceptible individual breathing normally. This corresponds to a risk of infection of 2.6%: a value much higher compared to that of the breathing scenario.

Figure 4 (Multimedia view) shows the results of the speaking scenario without room ventilation. Larger droplets are still small enough to have little inertia so that their horizontal velocity is quickly zeroed by drag once they exit from the breath cloud area of influence. As a consequence, their trajectories are mostly vertical rather than parabolic [see Fig. 4(a)]. The larger the droplets and the sooner they exit from the breath cloud, the shorter the horizontal distance traveled. In this scenario, for instance, supercritical droplets are deposited on the ground no further than 20 cm from the infected individual, as shown in Fig. 4(e), and their dispersion in the y direction is very limited. Smaller droplets can be transported further, and if their size is $> 20 - 30$ μm they are able to escape from the breath cloud by gravity at some point along their journey. Overall, the viral concentration associated with these droplets can be relatively high as shown in Fig. 4(b), but the horizontal distance traveled by them is small enough not to represent a serious threat to the safety of a susceptible individual maintaining a reasonable social distance [see Figs. 4(c) and 4(d)]. It is rather of concern the quantity of airborne viruses that may accumulate with time in a poorly ventilated environment and against which there is nothing social distancing can do. The deposition rate map in Fig. 4(f) is derived from the droplet deposition data in Fig. 4(e). The map is characterized by several local peaks due to the relatively limited number of droplets touching the ground (only 189 in this scenario) compared to the relatively large number of cells with which the ground is discretized. To obtain a more uniform and representative map, data in each cell is iteratively smoothed by averaging its value with that of the neighboring cells. The result of this process is shown in Fig. 4(f). To be noted that the random-walk turbulent dispersion model adopted randomly deviates the droplet trajectory so that they may fall either in

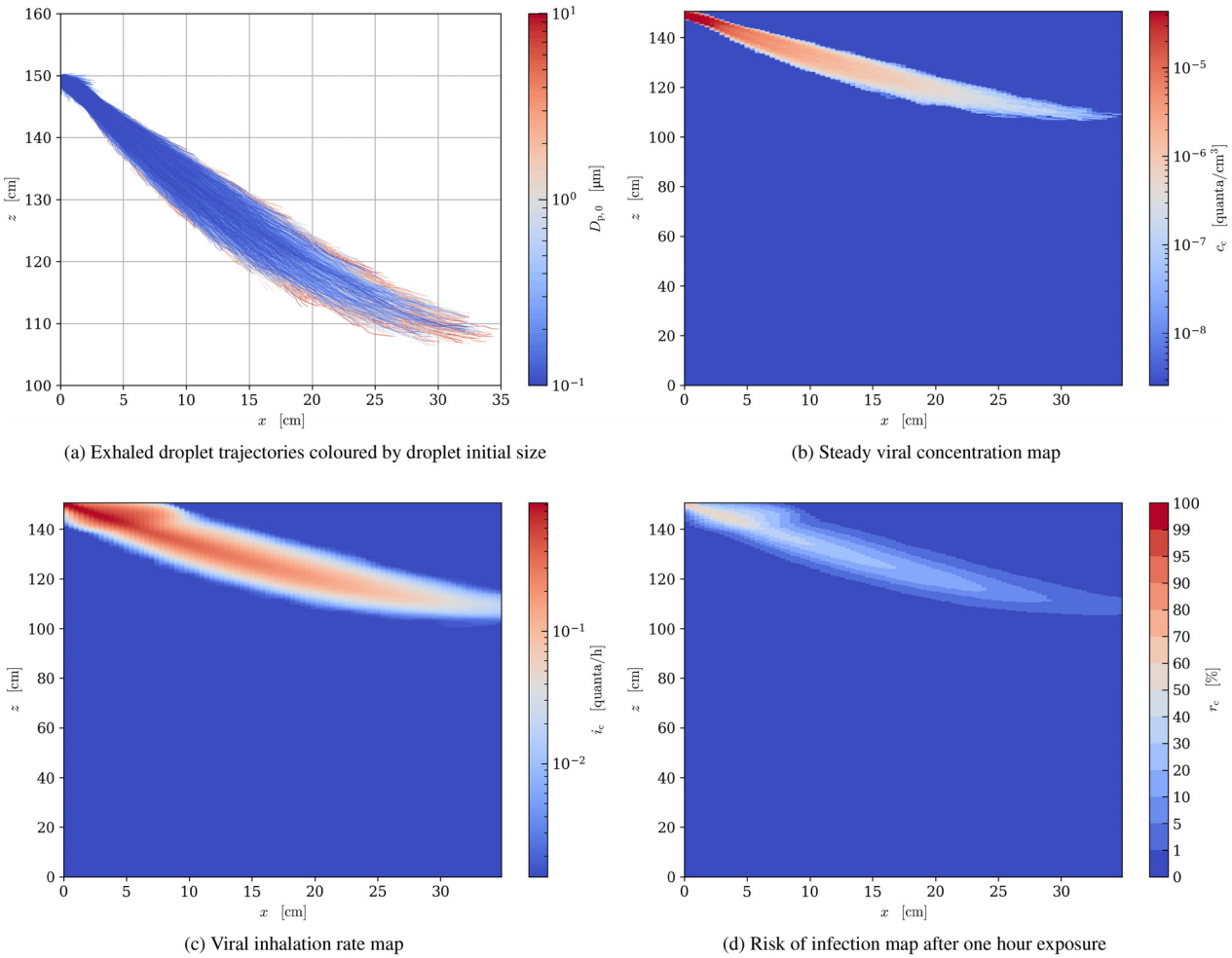

(a) Exhaled droplet trajectories coloured by droplet initial size

(b) Steady viral concentration map

(c) Viral inhalation rate map

(d) Risk of infection map after one hour exposure

FIG. 3. Results of the nose breathing scenario without room ventilation. Multimedia available online.

the y positive or negative half-plane indifferently. Considering the problem symmetry, all deposition coordinates are projected in the y-positive half-plane in Fig. 4(e) and the droplet viral content is split equally among the two half-planes to obtain the symmetrical plot in Fig. 4(f). To be also noted that the pixelated look that this and other maps might have is a consequence of the discretization used to create them. This effect is particularly evident where the extension of the map is limited in size. Nonetheless, finer discretizations would have led to less uniform and less significant maps, unless the number of simulations was increased exponentially.

The deposition rates in the figure are sufficient to justify a significant risk of fomite transmission in case an infected surface is touched and its viral load brought in contact with the airways of a susceptible individual. In total, the viral load deposited on the ground amounts to 3.8 quanta/h and from the simulations the infected area amounts to 57 cm^2. From Eq. (43), after one hour of exposure the average viral concentration on the ground amounts to 6.4×10^{-2} quanta/cm^2, and the risk of infection if a single square centimeter is touched and its viral load fully inhaled equals 6.2%. Further quantitative estimates can be derived easily from Eq. (37) as a function of the deposition time span, and thus of the actual viral concentration on the surface, and the extension of the contact. It is worth mentioning that the virus half-life on surfaces is generally much higher compared to air, and according to the data provided in Ref. 31 for SARS-CoV-2 the characteristic time associated with the virus titer decay on a surface can be as high as 10 h. This means a surface may still represent a non-negligible threat in view of fomite transmission even a few days after infection.

Trajectories are much different in the ventilated scenario shown in Fig. 5 (Multimedia view). Droplets are carried by the air stream, and having different terminal velocities depending on their size, they stratify in the vertical direction creating a compact front advancing in time as highlighted in Fig. 5(a) and in the multimedia material provided. As a result, the risk of infection [Fig. 5(b)] remains considerable also at larger distances from the infected individual, and at any height. A clear stratification is also apparent in the droplet deposition plot [Fig. 5(c)] where slightly smaller droplets are carried much further by the air flow before being deposited on the ground. The average deposition rate in Fig. 5(d) is lower compared to the previous non-ventilated case due to

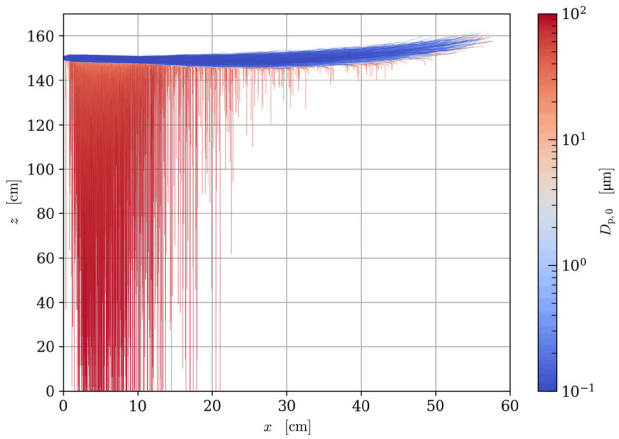

(a) Exhaled droplet trajectories coloured by droplet initial size

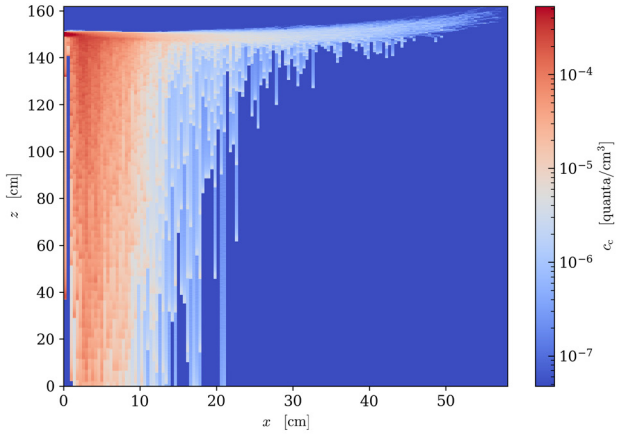

(b) Steady viral concentration map

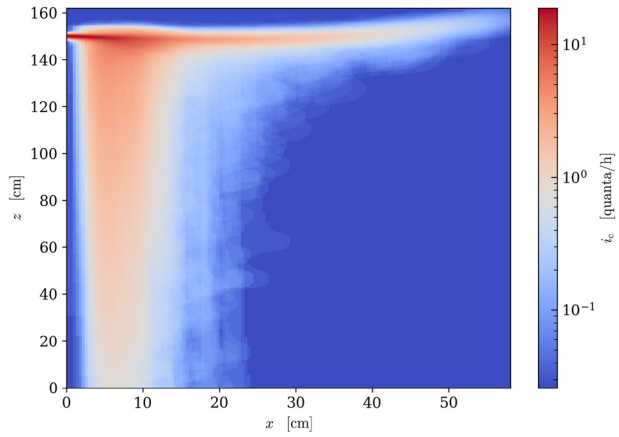

(c) Viral inhalation rate map

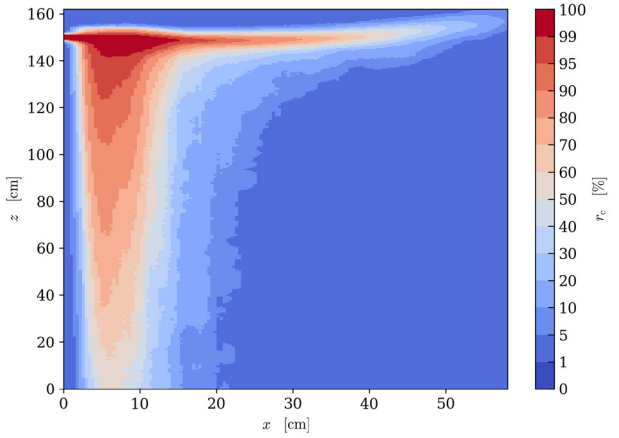

(d) Risk of infection map after one hour exposure

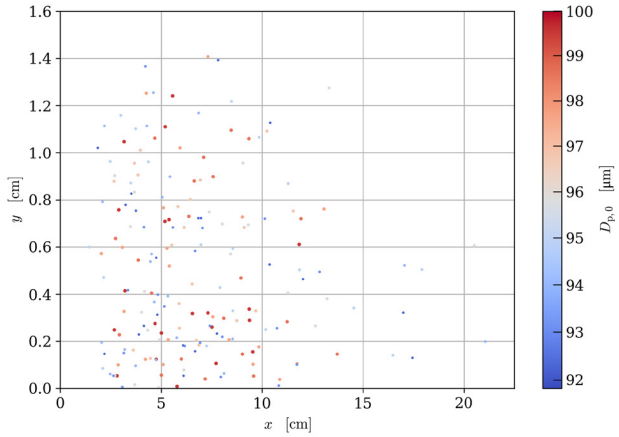

(e) Exhaled droplet ground deposition coloured by droplet initial size

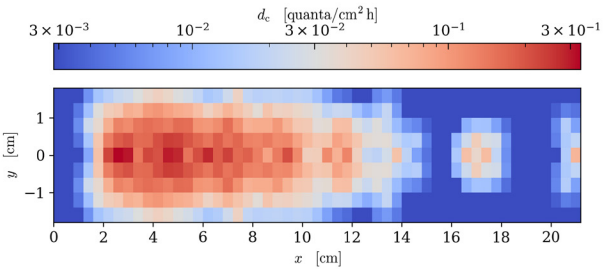

(f) Viral deposition rate at the ground

FIG. 4. Results of the speaking scenario without room ventilation. Multimedia available online.

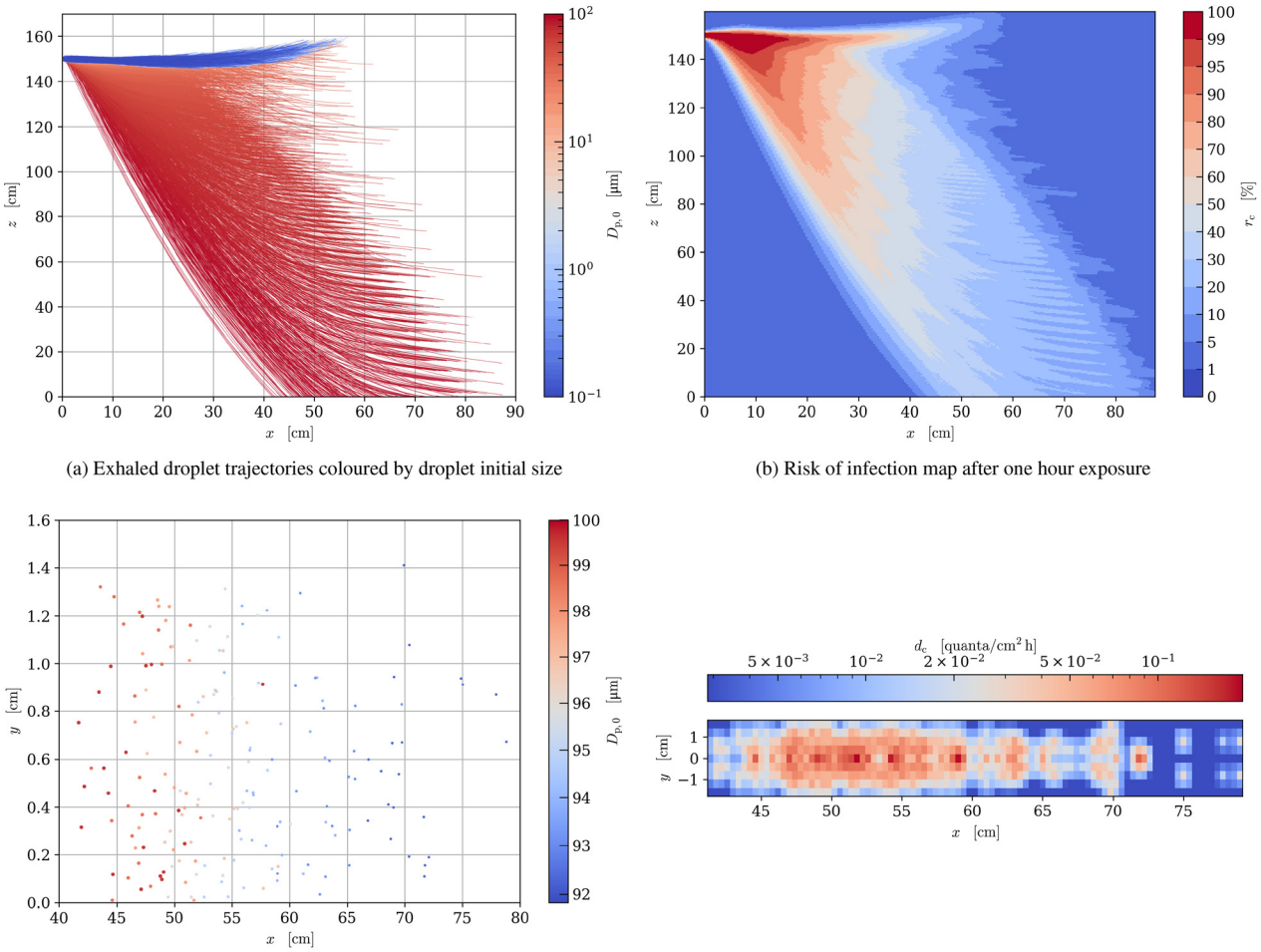

(a) Exhaled droplet trajectories coloured by droplet initial size

(b) Risk of infection map after one hour exposure

(c) Exhaled droplet ground deposition coloured by droplet initial size

(d) Viral deposition rate at the ground

FIG. 5. Results of the speaking scenario with room ventilation. Multimedia available online.

the larger area (110 cm^2 from the simulations) over which the same amount of virus is spread. Note that no droplet is deposited within a distance of 40 cm from the infected individual since the falling time of larger droplets is ≈ 8 s and the air velocity 5 cm/s. These results highlight the pros and the cons of ventilation. Ventilation, in fact, is generally associated with higher air change rates in a room, and as such it is most welcome in that it helps diluting the virus concentration lowering the risk of airborne transmission. On the other hand, if a susceptible individual accidentally finds himself downstream of an infected one, the chances of transmission by direct inhalation are largely increased. For what concerns fomite transmission, in the presence of ventilation the chance of inhaling viruses is higher due to the larger droplet dispersion on surfaces, but the risk of disease transmission is lower thanks to the greater virus dilution.

C. Coughing

Coughing, together with sneezing, is an isolated respiratory event characterized by the rapid exhalation of a large amount of droplets. This is reflected both in the values of the coefficient B in Table I, that for coughing is more than 300 times larger compared to speaking, and in the fivefold exhalation velocity reported in Table IV. Overall, the number of exhaled quanta associated with a single coughing event has been estimated in 172.8 in Table II. After the simulations, a critical diameter of ≈ 87.0 μm is found for both ventilation scenarios, a value slightly lower than the one found for speaking. This is justified by the direction of the exhalation which is tilted downward and thus favors droplet deposition. The quanta airborne fraction equals 9% of the total and amounts to 15.0 quanta per event. This suggests that, for what concerns the airborne viral load, one cough equals ≈ 20 min speaking. This quantity translates into an average airborne viral concentration in the room of $\approx 2.8 \times 10^{-8}$ quanta/cm^3 in the hour following the respiratory event according to Eq. (47), 1.5×10^{-2} quanta/h inhaled by a susceptible individual breathing normally, and a risk of infection of 1.5% after 1 h exposure.

Figures 6 and 7 (Multimedia views) show the results of the coughing scenarios. The latter including room ventilation, the former without. Figures 6(a) and 7(a) show the droplet trajectories.

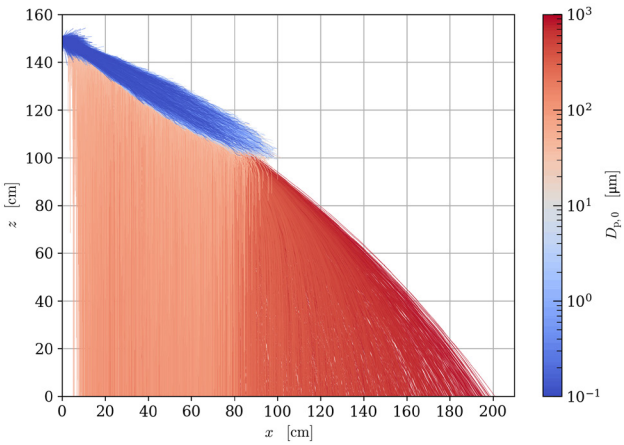

(a) Exhaled droplet trajectories coloured by droplet initial size

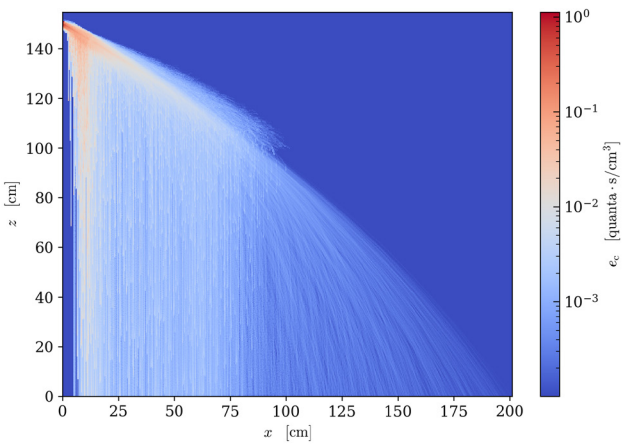

(b) Viral exposure map

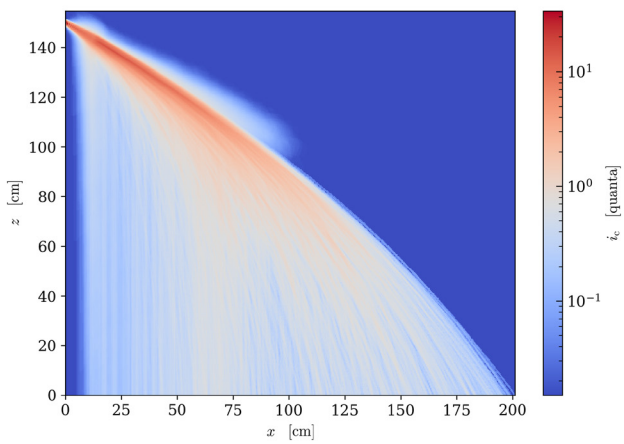

(c) Viral inhalation map

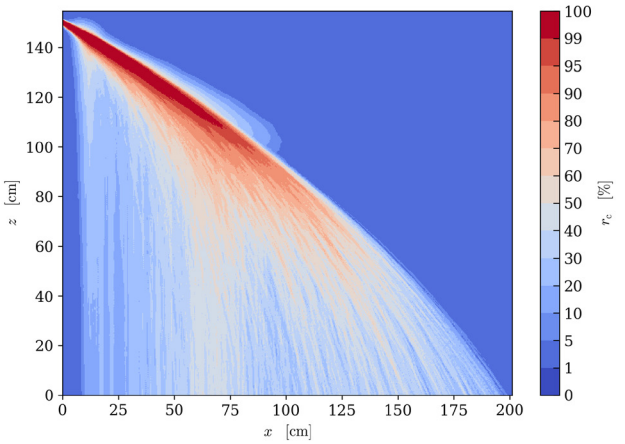

(d) Risk of infection map

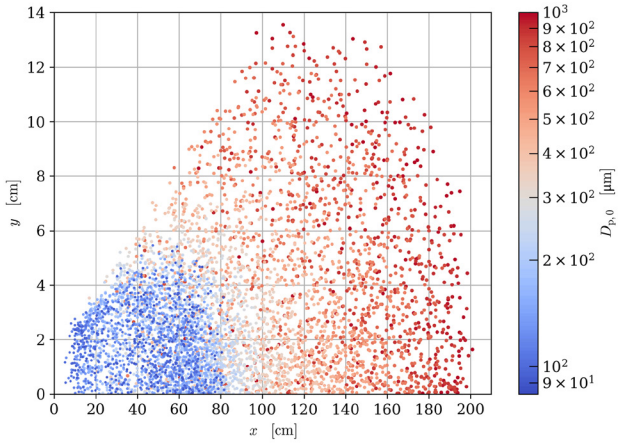

(e) Exhaled droplet ground deposition coloured by droplet initial size

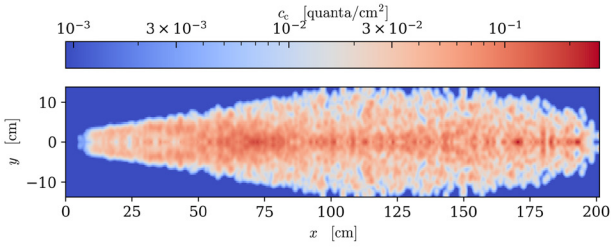

(f) Viral concentration at the ground one hour after the event

FIG. 6. Results of the coughing scenario without room ventilation. Multimedia available online.

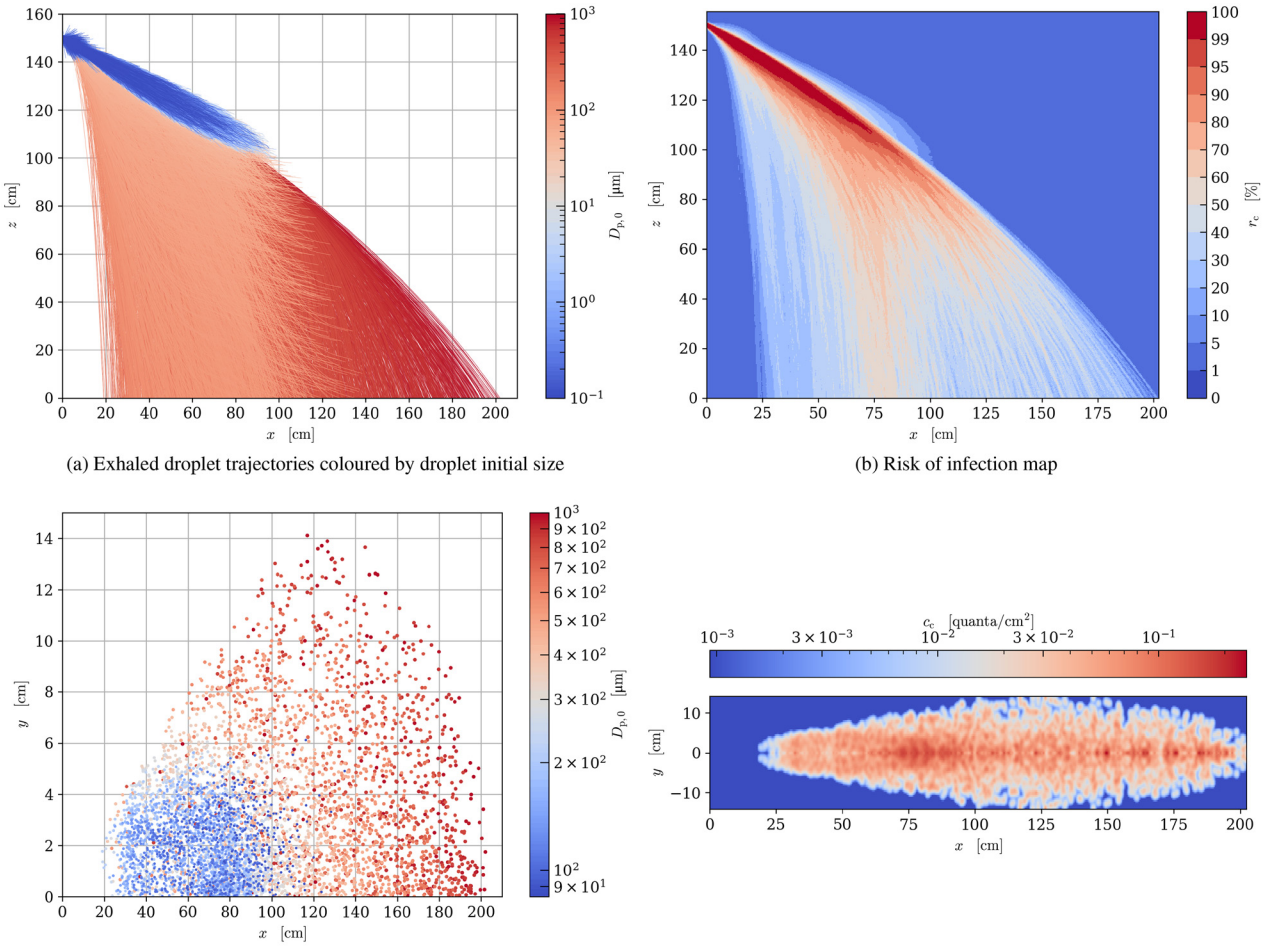

(a) Exhaled droplet trajectories coloured by droplet initial size

(b) Risk of infection map

(c) Exhaled droplet ground deposition coloured by droplet initial size

(d) Viral deposition at the ground one hour after the event

FIG. 7. Results of the coughing scenario with room ventilation. Multimedia available online.

Qualitatively, it is possible to discriminate between four types of droplet behavior: small droplets ($D_p < 20 - 30$ μm) whose trajectory is primarily due to their transport within the breath cloud and are affected by buoyancy, sub-critical intermediate droplets that remain airborne and whose trajectory is mostly governed by the local ventilation flow, supercritical intermediate droplets reaching the ground before evaporating and whose trajectory is affected by the local air flow to a lesser extent, and large droplets ($D_p > 300 - 400$ μm) whose trajectory tends to be parabolic and is not affected by air transport. Droplet dispersion on the ground follows a conic trace, as shown in Figs. 6(e) and 7(c), which is characterized by a slightly larger opening angle compared to that of the breath cloud ($\beta = 0.13$ vs $\beta = 0.11$). This shows how the impact of turbulent dispersion is marginal on supercritical droplets. Thanks to the larger velocities with whom droplets are exhaled and transported within the breath cloud, the horizontal distance reached is larger compared to previous scenarios, and with that also the risk of infection at a distance becomes meaningful. Small and intermediate size droplets form a rather compact front characterized by high viral exposure that fades with the distance [Figs. 6(b)] and is perceived up to 1 m distance and more in the case of ventilated scenario. Large droplets, mostly falling to the ground at a distance between 1 and 2 m from the infected individual, further extend the risk area [Figs. 6(d) and 7(b)]. The role of ventilation on the transport of intermediate droplets is apparent from Figs. 7(c) and 7(d) compared to their non-ventilated counterparts.

Despite the amount of quanta deposited on the ground after a cough is forty times larger (157.8 quanta) than that estimated after 1 h talk, much larger is also the area over which droplets are spread (0.40 m^2), so that after one hour from the coughing event the average viral concentration on the ground, estimated with Eq. (46), is just half (3.5×10^{-2} quanta/cm^2) and so is the risk of infection after touching and inhaling the viral content of one square centimeter (3.4%). To be considered that these are just average data, while the actual viral concentration on the floor varies significantly from place to place and peaks can be six times larger than that or more. Figure 6(f) provides a more detailed picture of this. In the ventilated scenario, the infected area is slightly reduced as small

droplets are transported further and none fall within 20 cm of the infected individual [see Figs. 6(e) and 7(c)].

D. Sneezing

Data in Table IV show that sneezing modeling is characterized by triple exhalation velocity compared to coughing and its direction is tilted upward. This means droplets are expected to cover a much wider range of distances in their trajectories. Furthermore, the coefficient B in Table I is 10 times larger, and so is the amount of virus exhaled that reaches 1727.9 quanta per event (see Table II). A critical diameter of ≈ 97.4 μm has been found in the simulations, meaning that the quanta airborne fraction is 10% of the total and equals 168.2 quanta per event. The average airborne viral concentration in the room in the hour following the respiratory event is as high as 3.1×10^{-7} quanta/cm^3, the quantity of airborne virus inhaled amounts to 1.7×10^{-1} quanta/h, and the risk of infection after one hour exposure spikes at 15.5%.

Figure 8 (Multimedia view) shows the results of the sneezing scenario without ventilation. What catches the eyes looking at the trajectories in Fig. 8(a) is the large horizontal extent covering a distance up to 6 m from the infected individual. Overall, results are qualitatively similar to those already shown for coughing where the different behavior of droplets of different size can be recognized, and the droplet dispersion in the y direction shown in Fig. 8(e) is of the same entity. The main differences are in the direction of the breath cloud, and in the tenfold quanta exhalation that, although dispersed over a much larger volume of space, translates into an increased viral exposure even at a large distance [Fig. 8(b)] and a risk of infection above 90% over most of the area covered by the droplet flow [Fig. 8(d)]. As a result, according to these values a susceptible individual eventually hit by the exhalations from a sneeze has a high chance of directly inhaling enough viruses to develop the infectious disease. These numbers may seem too large, and maybe they are considering the level of uncertainty on the information about the viral load in droplets and about the infectious dose that can be found in the sparse data available in the literature. Nonetheless, it is certainly true that in this scenario a distance of 6 m could at best be considered barely sufficient to avoid the risk of direct contagion.

Results of the ventilated scenario are omitted for brevity in that they only differ in the distance traveled by intermediate droplet in a similar fashion to what already seen in the coughing scenario.

To be noted how the maps in Fig. 8 appear less smooth compared to those obtained in previous scenarios, and the trajectories associated with the single droplets can be perceived in the maps, in particular for what concerns large droplets. Even though the number of droplet simulated is very high, in fact, this number is not enough to cover uniformly such a large portion of space. With the simulation of additional droplets the maps could be made smoother and a more gradual fading of the risk with distance would appear. The considerations made on the safety distance to be kept with respect to a sneezing infected individual, nonetheless, would not change significantly. The map that suffers the most from the limited number of droplets simulated is the one showing the viral concentration at the ground in Fig. 8(f) due to the small ratio between the number of droplets reaching the ground (5161 in this scenario) and the number of pixels with whom the ground is discretized. In order to obtain a more continuous and plausible map in the post-processing of Fig. 8(f) the cell size has been increased to 12 mm. The infected area reaches an extension of 3.24 m^2, with an average viral concentration at the ground 1 h after exposure of 4.3×10^{-2} quanta/cm^2, and a risk of infection of 4.2% in case the viral content of one square centimeter is inhaled. These values are similar to those already found for coughing since even though the viral load is tenfold, also the infected surface grows nearly proportionally.

E. Airborne and fomite transmission

The results shown so far in Sec. VI are very informative in that they provide an estimate for different infectious disease transmission routes.

As mentioned, maps on the x–z vertical plane are associated with direct inhalation transmission route for the various scenarios analyzed and, to the author's knowledge, they are a first attempt in the literature to provide spatial-dependent quantitative estimates for this route. The estimates given rely on the analytical model summarized in Sec. II. The scenarios investigated may either refer to a periodic respiratory event (e.g., breathing or speaking) where viruses are exhaled periodically in time generating a virus concentration field which is steady on average, or to an isolated respiratory event (e.g., coughing or sneezing) where viruses are exhaled over a short lapse of time.

Along with this, also airborne transmission needs to be accounted for. Following the Wells–Riley model and assuming a well-mixed environment, airborne transmission risk is easily computed. Nonetheless, it must be considered that in this case the risk of transmission depends on the airborne virus concentration in the environment, which is a quantity that changes with continuity in time. In particular, the airborne spatial concentration grows with time in the case of periodic event due to the progressive accumulation of airborne droplet nuclei, while it decays with time in the case of isolated event due to virus titer decay and the progressive dilution by ventilation. In order to match these results, that are clearly dependent on the exposure time, with those of the maps focusing on direct transmission where the concentration is either steady or the viral exposure limited in time, the average concentration associated with airborne transmission has been computed for the various scenarios for a given time lapse going from zero to 1 h, as mentioned in Sec. V. The resulting quantities have been added to the maps and are represented by the background value reported at the bottom of each color bar.

Even though airborne concentration is small compared to the peaks found in the maps, its relevance is connected to the fact that airborne transmission may occur over large exposure times and despite the social distance that may be kept. It is, thus, worth focusing on how the risk of airborne transmission does change with the exposure time along with periodic infectious exhalations or following an isolated respiratory event. This aspect is investigated in the current section.

The considerations just made also hold for fomite transmission since the average virus concentration on the surface depends on both the viral load discharged on it (either periodically or in a single event) and on the virus titer decay on the surface, i.e., on the time passed since the event. Further, the risk of infection depends on the extension of the surface touched and whose viral load is accidentally inhaled. In this case, of course, the well-mixed assumption only gives an estimate of the average risk, knowing that the concentration is not uniform in space as shown in the x–y ground maps provided. The ground concentration maps in Secs. VI B–VI D show the picture at a given moment in time, chosen as either 1 h from the beginning of a periodic event, or 1 h after an isolated event. By accepting the well-mixed hypothesis,

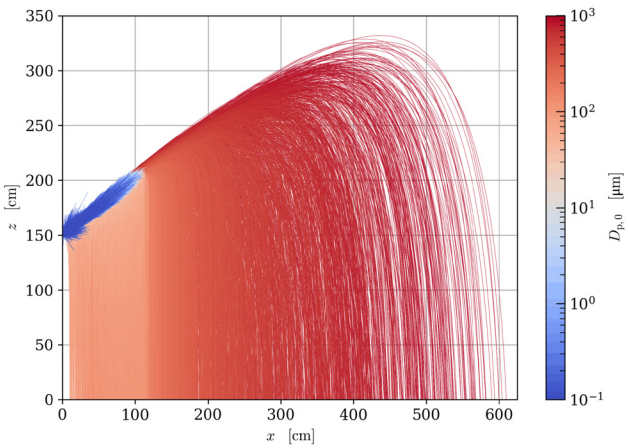

(a) Exhaled droplet trajectories coloured by droplet initial size

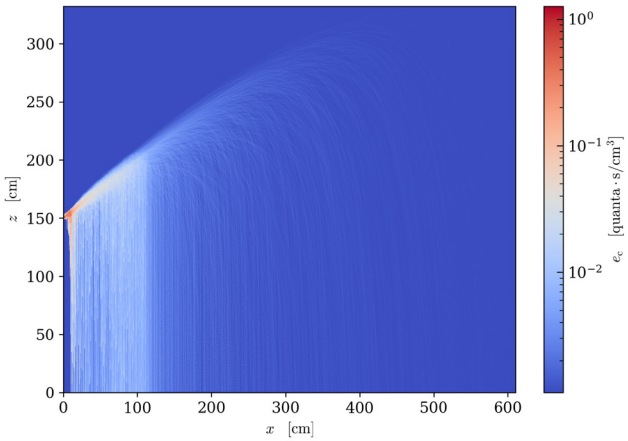

(b) Viral exposure map

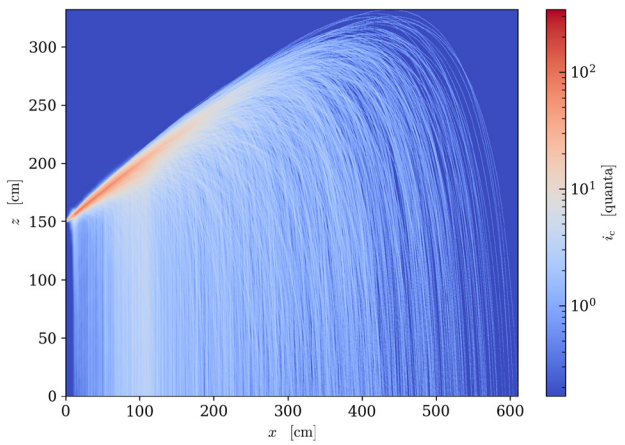

(c) Viral inhalation map

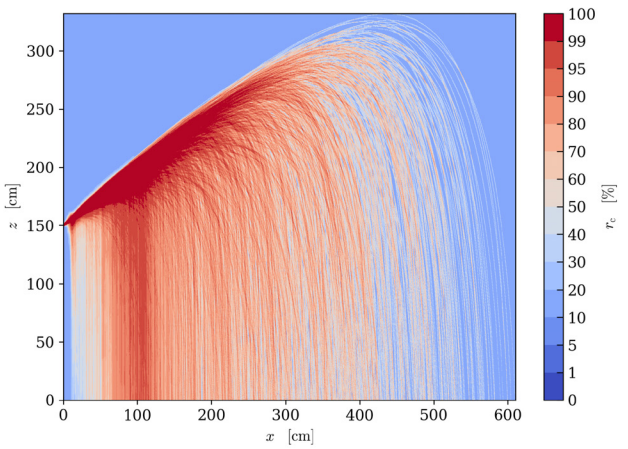

(d) Risk of infection map

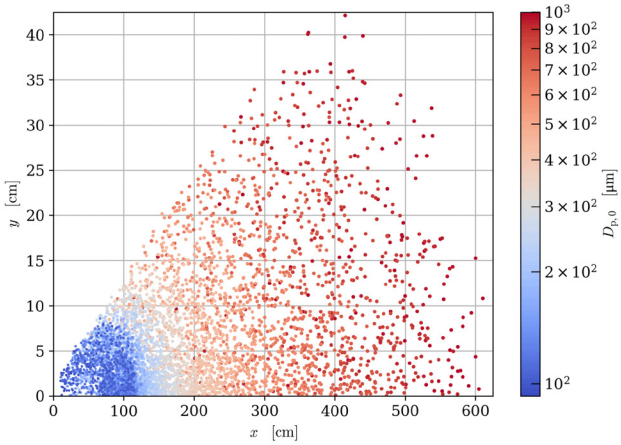

(e) Exhaled droplet ground deposition coloured by droplet initial size

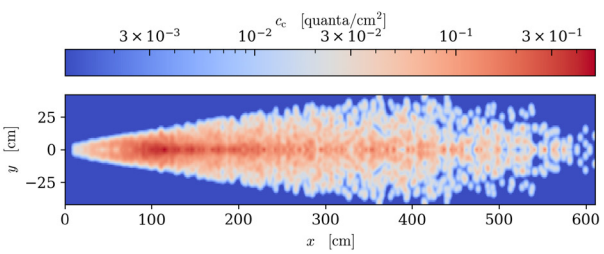

(f) Viral concentration at the ground one hour after the event

FIG. 8. Results of the sneezing scenario without room ventilation. Multimedia available online.

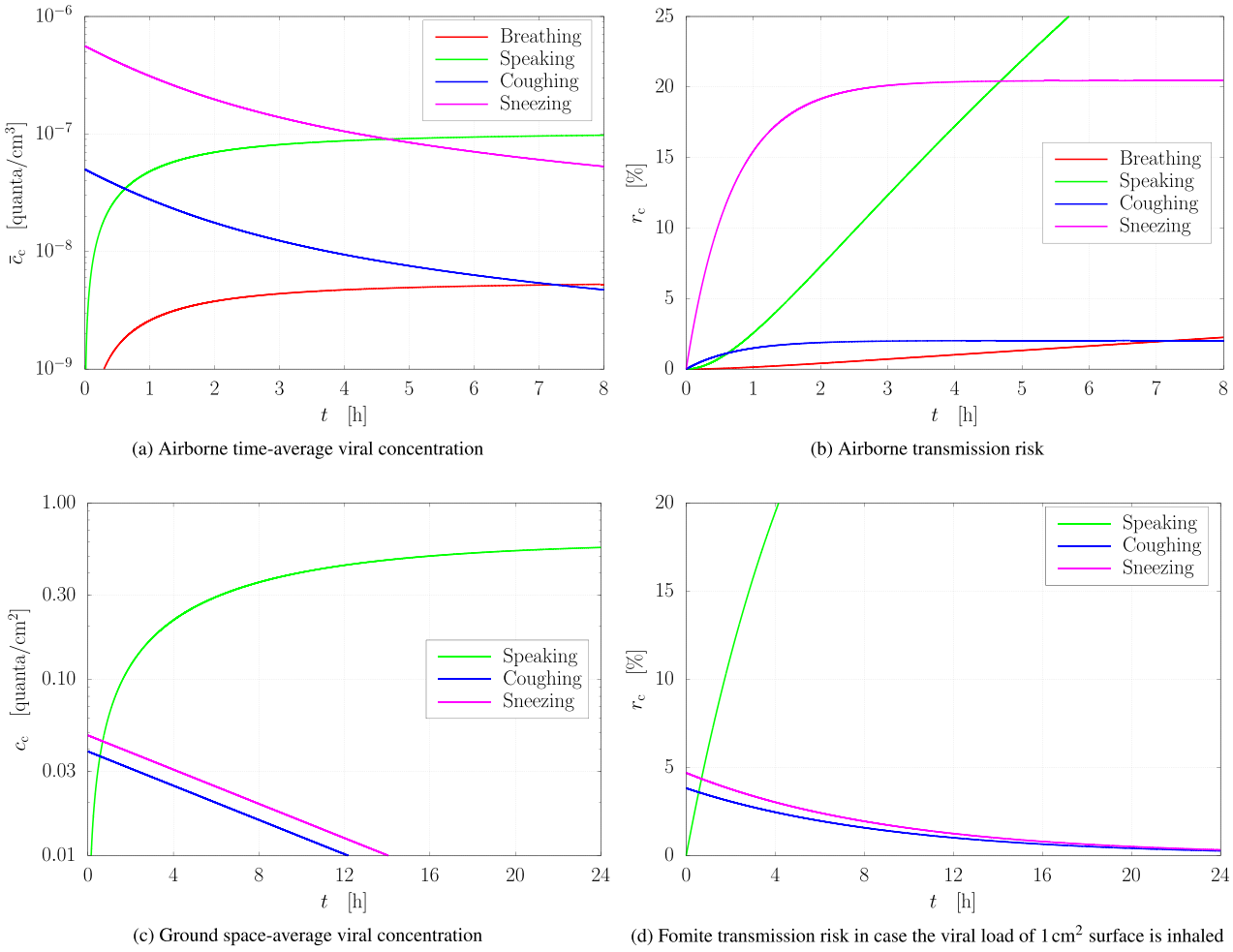

(a) Airborne time-average viral concentration

(b) Airborne transmission risk

(c) Ground space-average viral concentration

(d) Fomite transmission risk in case the viral load of 1 cm^2 surface is inhaled

FIG. 9. Airborne and fomite viral concentrations and transmission risk with time for the various scenarios investigated.

an estimate of how the average fomite transmission risk changes in time can be given.

The governing equations are those reported in Sec. V [Eqs. (42)–(47)]. These have been used to extract plots of the time-dependent virus concentration and the risk of infection associated with airborne and fomite transmission routes for the scenarios investigated in the current work. The results are shown in Fig. 9. Table V resumes the number of quanta exhaled associated with each respiratory event subdividing the data into airborne and deposited quantities as found in the simulations. For the evaluation of airborne concentration, the poorly ventilated office scenario described in Sec. V is assumed. Similarly, for the evaluation of ground concentration the infected surface areas found in the simulations for the non-ventilated cases are taken.

Figure 9(a) shows the airborne average viral concentrations a susceptible individual would be subject to while staying in an infected room for a certain amount of time. To be noted that, as the characteristic time is the same for all the events, the concentrations associated with periodic events show the same trend and scale linearly with the airborne quanta, and also those associated with isolated events decay with the same rate. Data in Fig. 9(a) are processed through Eqs. (35) and (37) to provide the risk plot in Fig. 9(b). While the airborne transmission risk associated with breathing or to a single cough is pretty much negligible, it is shown how sneezing and prolonged speaking in poorly ventilated environments may spark high risks of infection.

For the same reason noted above, also the decay rate of the viral concentration on the ground is the same for every respiratory event and amounts to approximately one order of magnitude every twenty

TABLE V. Airborne and deposited quanta exhaled for each type of respiratory event.

Respiratory Event	Airborne quanta	Deposited quanta	Infected surface
Breathing	2.31/h	0.00/h	
Speaking	42.80/h	3.81/h	57 cm^2
Coughing	15.02	157.77	4 048 cm^2
Sneezing	168.22	1559.66	32 430 cm^2

hours. Figure 9(c) shows the trends of the ground viral concentration in time for different respiratory events. These data are then recasted in terms of conditional risk of infection using Eq. (37) and assuming the viral load of a 1 cm^2 infected surface is inhaled. The two figures show that a small and comparable risk of fomite infection may follow from both coughing and sneezing: even though the viral load is high, it is spread over large surfaces. The risk associated with prolonged speaking instead may become relevant due to the limited area over which the virus is spread, at least under the hypothesis that the speaker does not move while speaking. Nonetheless, it must be considered that fomite infection risk may be largely limited adopting a proper behavior (e.g., with frequent hand washing and avoiding bringing the hands close to the airways), whereas the effectiveness of face masks against airborne transmission is only marginal.

F. Sensitivity analysis

The boundary conditions used in the previous scenarios are those resumed in Tables III and IV. In view of infection risk assessment, it is worth investigating to what extent the trajectories of the droplets are affected by the change in the simulation parameters. To do so, the horizontal distance traveled by a droplet before reaching the ground or before becoming airborne has been chosen as representative metric. Additional simulations are performed for each non-ventilated scenario in which the randomization elements described in Sec. II F are turned off, and droplets of different size are released from the breath cloud center ($\zeta = 0$) at the velocity peak time t_{pk}. In this way, the horizontal distance found is close to maximum. Simulations are then repeated by changing one parameter at a time over a range of $\pm 10\%$, where applicable, with respect to the values in the tables. All parameters are included in the analysis with the exception of the ambient ventilation that was set to zero in this analysis, and the times of the breathing function.

It is found that all parameters related to the droplet solid fraction and thermophysical properties are irrelevant. This is an expected results in that the behavior of large droplets is not affected by a solid fraction that is anyhow small, while airborne droplets are mostly transported by the breath cloud whatever their size and solid content. All quantities directly related to the local air density and the droplet evaporation rate (i.e., ambient pressure, temperature, and relative humidity) play a minor role only on the trajectories of large droplets, in particular for what concerns the sneezing scenario. Lower air densities in the ambient and slower evaporation rates, in fact, are associated with lower drag forces and larger droplet inertia, and translate into larger distances traveled. Nonetheless, small droplets have too little inertia to be affected significantly by the small change in density. The same occurs with the height at which the droplets are released: only large droplets characterized by nearly parabolic trajectories extend the range of the distance traveled when released from higher altitudes while smaller droplets are not affected by this parameter.

The most relevant impact on the droplet trajectories comes from parameters that are either directly related to the exhalation velocity (e.g., mouth diameter, exhaled volume, or initial velocity with respect to the cloud velocity) or to the rate at which the breath cloud velocity decreases with the distance (e.g., entrainment coefficient and momentum dissipation characteristic time). The latter mostly affect small droplets, the former large droplet trajectories. Furthermore, the breath cloud direction of course plays an important role on all droplet sizes.

A more detailed sensitivity analysis was carried out on these six parameters over larger ranges of variation. The results are shown in Fig. 10. Three droplet diameters are represented: one for droplets having nearly parabolic trajectories (1 mm), one for droplets that are fully transported by the breath cloud (10 μm), and one with an intermediate size so that the droplet quickly escapes the area of influence of the breath cloud but then tends to fall vertically being quickly damped by drag (100 μm). The word "mouth" in the captions refers both to mouth breathing and speaking scenarios since they share the same breath cloud modeling, whereas "nose" identifies nose breathing. The sensitivity to the mouth or nose opening diameter is reported in Fig. 10(a). Since the initial velocity scales with the square of the diameter this quantity has a major impact over large and intermediate droplets, whose distance traveled scales approximately with D_{mt}^{-1}. Small droplets are affected to a lesser extent since larger diameters are also associated with a slower velocity decay in the breath cloud with the distance. In this case, the distance traveled scales approximately with $D_{mt}^{-1/2}$. Figure 10(b) shows the sensitivity to the volume of air exhaled. Except for intermediate droplets where the impact may be larger, the distance traveled is shown to scale approximately with $V_{ex}^{1/2}$ for all droplets. Large droplets distance scales approximately with $||u_p||^{2/5}$ in Fig. 10(c), whereas smaller droplet trajectories are not affected by the initial velocity: their inertia, in fact, is so small that in any case they settle to the breath cloud velocity almost instantaneously. The larger is the entrainment coefficient, the more rapidly the velocity will fade within the breath cloud. This affects the distance traveled by small droplets that scales approximately as $\beta^{-2/5}$ in Fig. 10(d). The opposite occurs with momentum dissipation characteristic time. The momentum within the breath cloud, in fact, will be dissipated more slowly with a larger τ_{ds}. The distance traveled by small droplets is found to scale approximately with $\tau_{ds}^{1/3}$ from data in Fig. 10(e). Finally, Fig. 10(f) shows the change in the horizontal distance traveled by droplets with the direction of the exhalation. Small and intermediate size droplets owe their trajectory to the transport within the breath cloud. As such, the distance traveled shows a peak at an angle of zero degrees, or slightly below: this, in fact, is were the horizontal extension of the buoyant breathing cloud is maximum. For large droplets, instead, the maximum distance traveled is found at a $\approx 20^\circ$ angle for both coughing and sneezing scenarios. This value is close to the actual direction estimated for sneezing. The low value of this angle compared to the one that can be derived from the theory of kinematics for the maximum range in the motion of a body thrown with velocity u from a height H in a gravitational field,

$$\theta = \arccos\left(\sqrt{\frac{2gH + u^2}{2gH + 2u^2}}\right), \tag{48}$$

demonstrates that the trajectory of large respiratory droplets, although apparently parabolic, is still affected by drag in a non-negligible way.

VII. CONCLUSIONS

An analytical model recently developed by the authors[22] and simulating the transport and the evaporation process of respiratory droplets has been extensively used to replicate different scenarios and evaluate the risk of infectious disease transmission from an infected individual. Beside the governing equations, the analytical tool implements a two-dimensional unsteady model of the buoyant breath cloud,

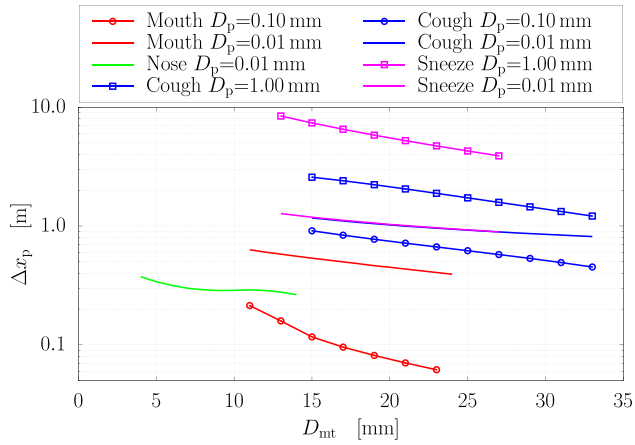

(a) Mouth/nose opening diameter

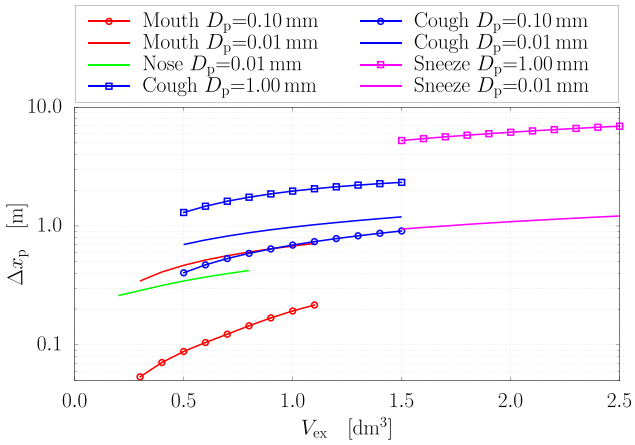

(b) Air volume exhaled per respiratory event

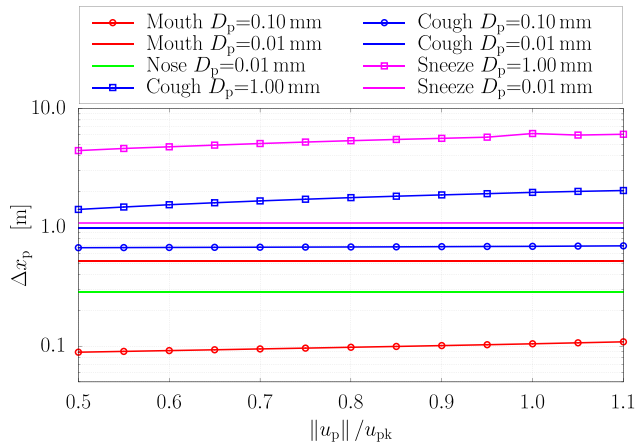

(c) Initial droplet to breath cloud velocity ratio

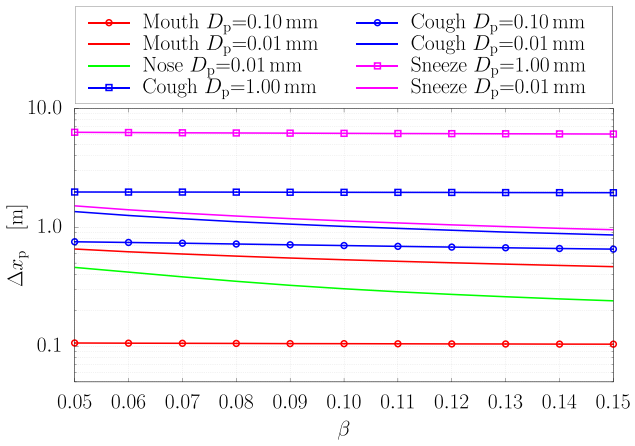

(d) Entrainment coefficient

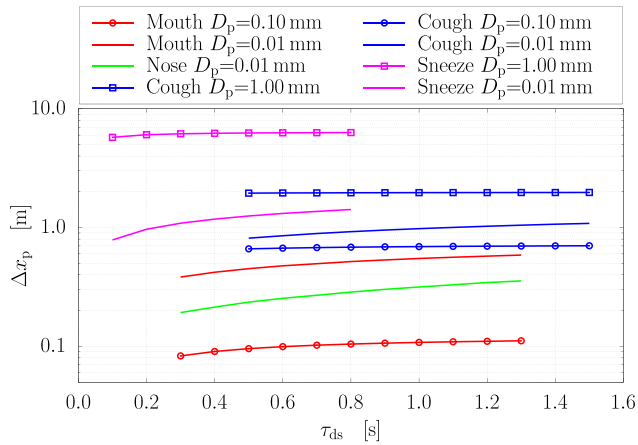

(e) Breath cloud momentum dissipation characteristic time

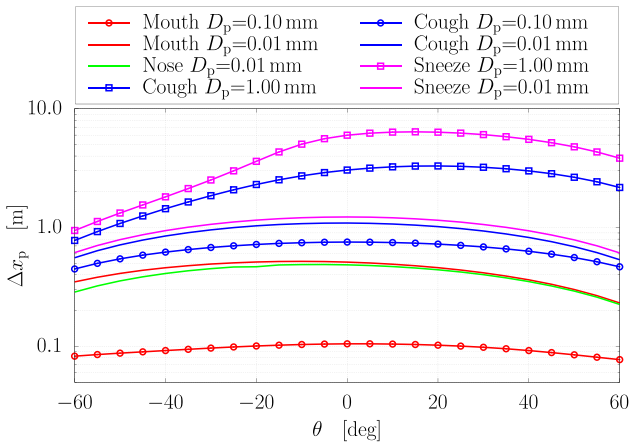

(f) Breath cloud exhalation direction over the horizontal

FIG. 10. Results of the sensitivity analysis: impact of the main simulation parameters on the horizontal distance Δx_p traveled by droplets of various size (see the line types) and for the different scenarios (see the line colors).

turbulent dispersion through a random walk approach, and randomized droplet exhalation. These stochastic features allowed statistical analyses on the droplet trajectory distribution to be performed based on the simulation of a large number of droplets. With additional information on the number and the size distribution of the exhaled droplets and on the viral content of the saliva, a viral load has been associated with each droplet. By analyzing the time evolution of the droplet trajectories, these data have been translated into practical viral concentration/exposure spatial maps of the neighborhood of the infected individual. A simple inhalation model was proposed to reformulate these maps in terms of quantity of viruses potentially inhaled by a susceptible individual and ultimately in terms of the resulting risk of infection. As such, the maps presented relate to the risk by direct inhalation route for an individual staying in the surroundings of an infected person for a certain amount of time. In addition, discriminating between the droplets remaining airborne and those falling to the ground by gravity, the risks associated with airborne and fomite transmission routes were quantified for a reference indoor environment using the Wells–Riley model. Virus accumulation maps on the ground were also derived from the simulation data.

The scenarios investigated include different periodic or isolated respiratory events such as mouth breathing, nose breathing, speaking, coughing, and sneezing. Simulations are repeated for the cases of quiescent and ventilated environment. A sensitivity analysis quantifying the effect of the variability of the scenario boundary conditions on droplet trajectories is also included. To the author's knowledge this is the first work where a similar analytical model is applied to systematically investigate different real-life scenarios quantifying the associated risks of transmission and being able to discriminate between the different transmission routes. The analytical model has the advantage of being cheap in terms of computational resources required and is very precise in evaluating the droplet trajectories compared to numerical methods that rely on a discretization in space and time that is necessarily approximate due to the scales of the problem at stake. On the contrary, the level of detail with whom the unsteady breath cloud air flow can be modeled using an analytical model, although elaborated, is necessarily lower compared to what can be achieved with expensive 3D unsteady numerical methods such as CFD. Concerning this, it is expected that in a real-life scenario smaller droplets will likely be subject to increased dispersion compared to what predicted in the present work. Another limit of the present study, at least for what concerns the post-processing of the results, is in the fact that in the literature there is little agreement on the quantity and the size distribution of the droplets exhaled during the different types of respiratory event. Further, the viral content in the saliva varies during the disease and also with the type of disease, and the infectious dose that is sufficient to transmit the illness is often known only approximately. For sure viral concentration, exposure, and inhalation maps will scale linearly with the total viral load delivered with the respiratory event, while assuming different droplet size distributions may weaken or strenghten the relative importance of certain areas in the maps.

All these uncertainties may affect the results from a quantitative point of view, meaning that the values presented in the maps might need to be shifted but not to be altered in their shape and with respect to the range of distances reached by the droplets. For the sake of presenting plausible results for potential risk scenarios, these uncertain quantities have been chosen at best, after a thorough analysis of the literature available on the topic for what concerns the recent SARS-CoV-2 pandemic.

The maps presented have been shown to be very informative, enabling the investigation of respiratory droplets and infectious disease transmission to a great degree of detail from a fluid mechanics perspective. Of course, any further medical or clinical observation is beyond the scope of the present work. The results allowed a comprehensive analysis on the behavior of droplets of different size, ranging from small ones mostly transported by the breath cloud, to intermediate size droplets that are easily carried by the local air flow associated with ventilation, and to large ones whose trajectory depends primarily on the initial velocity with whom they are exhaled. Ventilation has been shown to stratify intermediate size droplets creating compact advancing fronts of high risk areas that could be dangerous for a susceptible individual accidentally finding himself downstream of an infected one. This is apparent in the speaking scenario where otherwise the droplets would not be transported far from where they have been generated. The social distancing rule we all became acquainted with during the last pandemic have been shown to be sufficient only to prevent direct inhalation from a breathing or a speaking individual given that no strong ventilation is present. The large viral load and the large distances traveled by respiratory droplets associated with stronger respiratory events such as coughing and sneezing would call for an increased social distancing that in most environments is simply not possible to be kept. Moreover, these types of events also imply non-negligible risks of airborne and fomite infection in indoor settings. As a consequence, in these scenarios other means of prevention aimed at impeding large quantities of respiratory droplets from diffusing freely in the ambient, such as the use of face masks or paying attention to coughing or sneezeing covering the mouth with the sleeve, become of the utmost importance. Prolonged speaking can also induce large concentrations of virus to gradually accumulate in a small poorly ventilated indoor environment thus fostering airborne transmission, while normal breathing is associated with minor, although non fully negligible, levels of risk.

AUTHOR DECLARATIONS

Conflict of Interest

The authors have no conflicts to disclose.

Author Contributions

Marco Cavazzuti: Conceptualization (lead); Data curation (lead); Formal analysis (lead); Funding acquisition (lead); Investigation (lead); Methodology (lead); Project administration (equal); Resources (equal); Software (lead); Supervision (equal); Validation (lead); Visualization (lead); Writing – original draft (lead); Writing – review & editing (lead). **Paolo Tartarini:** Funding acquisition (supporting); Project administration (equal); Resources (equal); Supervision (equal).

DATA AVAILABILITY

The data that support the findings of this study are available from the corresponding author upon reasonable request.

NOMENCLATURE

b	Distance from centerline (m)
$\mathscr{B}$	Droplet size PDF (1/m)
C_d	Drag coefficient

c_c	Viral concentration ($1/m^3$; $1/m^2$)
c_p	Specific heat at constant pressure (J/kg K)
$\mathscr{D}$	Drag force (N)
D	Diameter (m)
D_v	Mass diffusivity (m^2/s)
d_c	Viral deposition rate ($1/m^2$ s)
e_c	Viral exposure (s/m^3)
$\mathbf{g}$	Gravitational acceleration (m^2/s)
H	Height (m)
h_{lt}	Latent heat of vaporization (J/kg)
i_c	Viral inhalation
$\bar{I}$	Average infectious dose
$\mathscr{I}$	Infectious dose PDF
K	Evaporation rate (m^2/s^2)
k	Turbulent kinetic energy (m^2/s^2)
M	Molar mass (kg/kmol)
$\dot{m}$	Mass flow rate (kg/s)
N	Number
Nu	Nusselt number
P	Momentum (Ns)
p	Pressure (Pa)
Q	Quanta
R	Specific gas constant (J/kg K)
r	Radius or radial distance (m)
r_c	Risk of infection
S	Surface (m^2)
Sh	Sherwood number
$\mathbf{s}$	Position (m)
T	Temperature (K)
t	Time (s)
$\mathbf{u}$	Velocity (m/s)
$\mathbf{u}'$	Velocity fluctuation (m/s)
V	Volume (m^3)
$\mathscr{W}$	Weight force (N)
y	Molar fraction
z	Vertical direction (m)

Greek symbols

β	Entrainment coefficient
γ	Cloud velocity scaling factor
ε	Turbulent dissipation rate (m^2/s^3)
ζ	Centerline dimensionless distance
$\boldsymbol{\eta}$	Normal distributed random vector
θ	Breath cloud direction (rad)
λ	Thermal conductivity (W/mK)
ξ	Radial dimensionless distance
ρ	Density (kg/m^3)
τ	Characteristic time(s)
φ	Volume fraction
ω	Mass fraction

Subscripts

a	Dry air
ab	Airborne
ac	Air change
avg	Average
c	Cell
D	Exhaled droplets
d	Drag
ds	Dissipation
e	Evaporation
ep	Exposure
ex	Exhalation
gr	Ground
hl	Half-life
in	Inhalation
lq	Liquid fraction
m	Humid air mixture
max	Maximum
min	Minimum
mt	Mouth
p	Particle or droplet
pk	Peak
pr	Period
r	Relative
rm	Room
s	Particle or droplet surface
sl	Solid fraction
st	Steady
sv	Saliva
t	Terminal
V	Exhaled viruses
v	Water vapor
∞	Ambient condition
0	Initial condition

REFERENCES

[1]H. Motamedi, M. Shirzadi, Y. Tominaga, and P. A. Mirzaei, "CFD modeling of airborne pathogen transmission of COVID-19 in confined spaces under different ventilation strategies," Sustainable Cities Soc. **76**, 103397 (2022).

[2]L. Borro, L. Mazzei, M. Raponi, P. Piscitelli, A. Miani, and A. Secinaro, "The role of air conditioning in the diffusion of SARS-CoV-2 in indoor environments: A first computational fluid dynamic model, based on investigations performed at the Vatican State Children's Hospital," Environ. Res. **193**, 110343 (2021).

[3]D. E. Ramayo and S. F. Corzo, "Airborne transmission risk in urban buses: A computational fluid dynamics study," Aerosol Air Qual. Res. **22**, 210334 (2022).

[4]V. Vuorinen, M. Aarnio, M. Alava, V. Alopaeus, N. Atanasova, M. Auvinen, N. Balasubramanian, H. Bordbar, P. Erästö, R. Grande, N. Hayward, A. Hellsten, S. Hostikka, J. Hokkanen, O. Kaario, A. Karvinen, I. Kivistö, M. Korhonen, R. Kosonen, J. Kuusela, S. Lestinen, E. Laurila, H. Nieminen, P. Peltonen, J. Pokki, A. Puisto, P. Råback, H. Salmenjoki, T. Sironen, and M. Österberg, "Modelling aerosol transport and virus exposure with numerical simulations in relation to SARS-CoV-2 transmission by inhalation indoors," Saf. Sci. **130**, 104866 (2020).

[5]G. Busco, S. R. Yang, J. Seo, and Y. A. Hassan, "Sneezing and asymptomatic virus transmission," Phys. Fluids **32**, 073309 (2020).

[6]B. Stiehl, R. Shrestha, S. Schroeder, J. Delgado, A. Bazzi, J. Reyes, M. Kinzel, and K. Ahmed, "The effect of relative air humidity on the evaporation timescales of a human sneeze," AIP Adv. **12**, 075210 (2022).

[7]T. Dbouk and D. Drikakis, "On respiratory droplets and face masks," Phys. Fluids **32**, 063303 (2020).

[8]C. Cravero and D. Marsano, "Simulation of COVID-19 indoor emissions from coughing and breathing with air conditioning and mask protection effects," Indoor Built Environ. **31**, 1242–1261 (2022).

[9]M. Puglia, F. Ottani, N. Morselli, S. Pedrazzi, G. Allesina, A. Muscio, A. Cossarizza, and P. Tartarini, "Airborne pathogens diffusion: A comparison

between tracer gas and pigmented aerosols for indoor environment analysis," Heliyon **10**, e26076 (2024).
[10]R. Albertin, G. Pernigotto, and A. Gasparella, "A Monte Carlo assessment of the effect of different ventilation strategies to mitigate the COVID-19 contagion risk in educational buildings," Indoor Air **2023**, 9977685.
[11]R. Mokhtari and M. H. Jahangir, "The effect of occupant distribution on energy consumption and COVID-19 infection in buildings: A case study of university building," Build. Environ. **190**, 107561 (2021).
[12]B. Wang, A. Zhang, J. L. Sun, H. Liu, J. Hu, and L. X. Xu, "Study of SARS transmission via liquid droplets in air," J. Biomech. Eng. **127**, 32–38 (2005).
[13]D. Parienta, L. Morawska, G. R. Johnson, Z. D. Ristovski, M. Hargreaves, K. Mengersen, S. Corbett, C. Y. H. Chao, Y. Li, and D. Katoshevski, "Theoretical analysis of the motion and evaporation of exhaled respiratory droplet of mixed composition," J. Aerosol Sci. **42**, 1–10 (2011).
[14]X. Xie, Y. Li, A. Chwang, P. Ho, and W. Seto, "How far droplets can move in indoor environments—Revisiting the Wells evaporation-falling curve," Indoor Air **17**, 211–225 (2007).
[15]W. Chen, N. Zhang, J. Wei, H.-L. Yen, and Y. Li, "Short-range airborne route dominates exposure of respiratory infection during close contact," Build. Environ. **176**, 106859 (2020).
[16]V. V. Baturin, *Fundamentals of Industrial Ventilation* (Pergamon Press, Oxford, 1972).
[17]J. Redrow, S. Mao, I. Celik, J. Posada, and Z.-G. Feng, "Modeling the evaporation and dispersion of airborne sputum droplets expelled from a human cough," Build. Environ. **46**, 2042–2051 (2011).
[18]J. Wei and Y. Li, "Enhanced spread of expiratory droplets by turbulence in a cough jet," Build. Environ. **93**, 86–96 (2015).
[19]S. Chan, K. Lee, and J. Lee, "Numerical modelling of horizontal sediment-laden jets," Environ. Fluid Mech. **14**, 173–200 (2014).
[20]L. Bourouiba, E. Dehandschoewercker, and J. Bush, "Violent expiratory events: On coughing and sneezing," J. Fluid Mech. **745**, 537–563 (2014).
[21]S. Balachandar, S. Zaleski, A. Soldati, G. Ahmadi, and L. Bourouiba, "Host-to-host airborne transmission as a multiphase flow problem for science-based social distance guidelines," Int. J. Multiphase Flow **132**, 103439 (2020).
[22]M. Cavazzuti and P. Tartarini, "Transport and evaporation of exhaled respiratory droplets: An analytical model," Phys. Fluids **35**, 103327 (2023).
[23]J. P. Duguid, "The size and the duration of air-carriage of respiratory droplets and droplet-nuclei," J. Hyg. **244**, 471–479 (1946).
[24]C. Y. H. Chao, M. P. Wan, L. Morawska, G. R. Johnson, Z. D. Ristovski, M. Hargreaves, K. Mengersen, S. Corbett, Y. Li, X. Xie, and D. Katoshevski, "Characterization of expiration air jets and droplet size distributions immediately at the mouth opening," J. Aerosol Sci. **40**, 122–133 (2009).
[25]L. Morawska, G. R. Johnson, Z. D. Ristovski, M. Hargreaves, K. Mengersen, S. Corbett, C. Y. H. Chao, Y. Li, and D. Katoshevski, "Size distribution and sites of origin of droplets expelled from the human respiratory tract during expiratory activities," J. Aerosol Sci. **40**, 256–269 (2009).
[26]M. Alsved, A. Matamis, R. Bohlin, M. Richter, P.-E. Bengtsson, C.-J. Fraenkel, P. Medstrand, and J. Löndahl, "Exhaled respiratory particles during singing and talking," Aerosol Sci. Technol. **54**, 1245–1248 (2020).
[27]L. Bourouiba, "Fluid dynamics of respiratory infectious diseases," Annu. Rev. Biomed. Eng. **23**, 547–577 (2021).
[28]K.-W. To, O.-Y. Tsang, C.-Y. Yip, K.-H. Chan, T.-C. Wu, J.-C. Chan, W.-S. Leung, T.-H. Chik, C.-C. Choi, D. Kandamby, D. Lung, A. Tam, R.-S. Poon, A.-F. Fung, I.-N. Hung, V.-C. Cheng, J.-W. Chan, and K.-Y. Yuen, "Consistent detection of 2019 novel coronavirus in saliva," Clin. Infect. Dis. **71**, 841–843 (2020).
[29]Y. Pang, D. Zang, P. Yang, L. Poon, and Q. Wang, "Viral load of SARS-CoV-2 in clinical samples," Lancet Infect. Dis. **20**, 411–412 (2020).
[30]J. M. Kolinski and T. M. Schneider, "Superspreading events suggest aerosol transmission of SARS-CoV-2 by accumulation in enclosed spaces," Phys. Rev. E **103**, 033109 (2021).
[31]N. van Doremalen, T. Bushmaker, D. H. Morris, M. G. Holbrook, A. Gamble, B. N. Williamson, A. Tamin, J. L. Harcourt, N. J. Thornburg, S. I. Gerber, J. O. Lloyd-Smith, E. de Wit, and V. J. Munster, "Aerosol and surface stability of SARS-CoV-2 as compared with SARS-CoV-1," N. Engl. J. Med. **382**, 1564–1567 (2020).
[32]G. Buonanno, L. Stabile, and L. Morawska, "Estimation of airborne viral emission: Quanta emission rate of SARS-CoV-2 for infection risk assessment," Environ. Int. **141**, 105794 (2020).
[33]J. Pantelic and K. W. Tham, "Assessment of the mixing air delivery system ability to protect occupants from the airborne infectious disease transmission using Wells–Riley approach," HVACR Res. **18**, 562–574 (2012).
[34]E. C. Riley, G. Murphy, and R. L. Riley, "Airborne spread of measles in a suburban elementary school," Am. J. Epidemiol. **107**, 421–432 (1978).
[35]W. F. Wells, *Airborne Contagion and Air Hygiene: An Ecological Study of Droplet Infections* (Harvard University Press, Cambridge, 1955).
[36]"REHVA COVID-19 guidance document: How to operate and use building services in order to prevent the spread of the coronavirus disease (COVID-19) virus (SARS-CoV-2) in workplaces," Technical Report (Federation of European Heating, Ventilation and Air Conditioning Associations, 2020).
[37]F. Bozzoli, L. Cattani, and S. Rainieri, "Effect of wall corrugation on local convective heat transfer in coiled tubes," Int. J. Heat Mass Transfer **101**, 76–90 (2016).
[38]S. Elgobashi and G. C. Truesdell, "Direct simulation of particle dispersion in a decaying isotropic turbulence," J. Fluid Mech. **242**, 655–700 (1992).
[39]E. Cunningham, "On the velocity of steady fall of spherical particles through fluid medium," Proc. R. Soc. A **83**, 357–365 (1910).
[40]W. E. Ranz and W. R. Marshall, "Evaporation from drops, Part I," Chem. Eng. Prog. **48**, 141–146 (1952).
[41]W. E. Ranz and W. R. Marshall, "Evaporation from drops, Part II," Chem. Eng. Prog. **48**, 173–180 (1952).
[42]F.-M. Raoult, "Loi générale des tensions de vapeur des dissolvants," C. R. Hebd. Seances Acad. Sci. **104**, 1430–1433 (1887).
[43]J. K. Gupta, C.-H. Lin, and Q. Chen, "Flow dynamics and characterization of a cough," Indoor Air **19**, 517–525 (2009).
[44]J. Gupta, C.-H. Lin, and Q. Chen, "Characterizing exhaled airflow from breathing and talking," Indoor Air **20**, 31–39 (2010).
[45]B. Wang, H. Wu, and X.-F. Wan, "Transport and fate of human expiratory droplets—A modeling approach," Phys. Fluids **32**, 083307 (2020).
[46]J. Smolík, L. Džumbová, J. Schwarz, and M. Kulmala, "Evaporation of ventilated water droplet: Connection between heat and mass transfer," J. Aerosol Sci. **32**, 739–748 (2001).
[47]S. Chaudhuri, S. Basu, P. Kabu, V. R. Unni, and A. Saha, "Modeling the role of respiratory droplets in Covid-19 type pandemics," Phys. Fluids **32**, 063309 (2020).
[48]H. Wang, Z. Li, X. Zhang, L. Zhu, Y. Liu, and S. Wang, "The motion of respiratory droplets produced by coughing," Phys. Fluids **32**, 125102 (2020).
[49]C. P. Cummins, O. J. Ajayi, F. V. Mehendale, R. Gabl, and I. M. Viola, "The dispersion of spherical droplets in source-sink flows and their relevance to the COVID-19 pandemic," Phys. Fluids **32**, 083302 (2020).
[50]N. H. L. Leung, D. Chu, E. Shiu, K.-H. Chan, J. McDevitt, B. J. Hau, H.-L. Yen, Y. Li, D. K. M. Ip, J. S. M. Peiris, W.-H. Seto, G. Leung, D. Milton, and B. Cowling, "Respiratory virus shedding in exhaled breath and efficacy of face masks," Nat. Med. **26**, 676–680 (2020).
[51]R. Alford, J. Kasel, P. Gerone, and V. Knight, "Human influenza resulting from aerosol inhalation," Proc. Soc. Exp. Biol. Med. **122**, 800–804 (1966).
[52]S. Asadi, A. Wexler, C. Cappa, S. Barreda, N. Bouvier, and W. Ristenpart, "Aerosol emission and superemission during human speech increase with voice loudness," Sci. Rep. **9**, 2348 (2019).
[53]P. Bahl, C. Doolan, C. de Silva, A. A. Chughtai, L. Bourouiba, and C. R. MacIntyre, "Airborne or droplet precautions for health workers treating coronavirus disease 2019?," J. Infect. Dis. **225**, 1561–1568 (2020).
[54]J. Tang, A. Nicolle, C. Klettner, J. Pantelic, L. Wang, A. Suhaimi, A. Tan, G. Ong, R. Su, C. Sekhar, D. Cheong, and K. Tham, "Airflow dynamics of human jets: Sneezing and breathing—Potential sources of infectious aerosols," PLoS One **8**, e59970 (2013).
[55]H. Li, F. W. Leong, G. Xu, Z. Ge, C. W. Kang, and K. H. Lim, "Dispersion of evaporating cough droplets in tropical outdoor environment," Phys. Fluids **32**, 113301 (2020).

[56]J. Wang, F. Dalla Barba, A. Roccon, G. Sardina, A. Soldati, and F. Picano, "Modelling direct virus exposure risk associated with respiratory events," J. R. Soc. Interface **19**, 20210819 (2022).
[57]B. Kumar, N. Kashyap, A. Avinash, R. Chevvuri, M. Sagar, and K. Shrikant, "The composition, function and role of saliva in maintaining oral health: A review," Int. J. Contemp. Dent. Med. Rev. **2017**, 011217.
[58]M. Abkarian, S. Mendez, N. Xue, F. Yang, and H. Stone, "Speech can produce jet-like transport relevant to asymptomatic spreading of virus," Proc. Natl. Acad. Sci. U. S. A. **117**, 25237–25245 (2020).
[59]C. Xu, P. Nielsen, L. Liu, R. Jensen, and G. Gong, "Human exhalation characterization with the aid of schlieren imaging technique," Build. Environ. **112**, 190–199 (2017).
[60]E. Bjørn and P. Nielsen, "Dispersal of exhaled air and personal exposure in displacement ventilated rooms," Indoor Air **12**, 147–164 (2002).
[61]T. Foat, B. Higgins, C. Abbs, T. Maishman, S. Coldrick, A. Kelsey, M. Ivings, S. Parker, and C. Noakes, "Modelling the effect of temperature and relative humidity on exposure to SARS-CoV-2 in a mechanically ventilated room," Indoor Air **32**, e13146 (2022).